

Unveiling the regulatory role of GRP7 in ABA signal-mediated mRNA translation efficiency regulation

Received: 12 January 2024

Accepted: 15 April 2025

Published online: 26 April 2025

 Check for updates

Jing Zhang^{1,2,10}, Wenna Shao^{3,10}, Yongxin Xu^{1,2,10}, Fa'an Tian^{2,4}, Jinchao Chen^{1,2}, Dongzhi Wang¹, Xuelei Lin¹, Chongsheng He⁵, Xiaofei Yang^{6,7}, Dorothee Staiger⁸, Yiliang Ding⁶, Xiang Yu³✉ & Jun Xiao^{1,2,9}✉

Abscisic acid (ABA) is a crucial phytohormone involved in plant growth and stress responses. While the transcriptional regulation triggered by ABA is well-documented, its effects on translational regulation have been less studied. Through Ribo-seq and RNA-seq analyses, we find that ABA treatment not only influences gene expression at the mRNA level but also significantly impacts mRNA translation efficiency (TE) in *Arabidopsis thaliana*. ABA inhibits global mRNA translation via its core signaling pathway, which includes ABA receptors, protein phosphatase 2Cs (PP2Cs), and SNF1-related protein kinase 2s (SnRK2s). Upon ABA treatment, Glycine-rich RNA-binding proteins 7 and 8 (GRP7&8) protein levels decrease due to both reduced mRNA level and decreased TE, which diminishes their association with polysomes and leads to a global decline in mRNA TE. The absence of GRP7&8 results in a global impairment of ABA-regulated translational changes, linking ABA signaling to GRP7-dependent modulation of mRNA translation. The regulation of GRP7 on TE relies significantly on its direct binding to target mRNAs. Moreover, mRNA translation efficiency under drought stress is partially dependent on the ABA-GRP7&8 pathways. Collectively, our study reveals GRP7's role downstream of SnRK2s in mediating translation regulation in ABA signaling, offering a model for ABA-triggered multi-route regulation of environmental adaptation.

Abscisic acid (ABA) is a crucial phytohormone that regulates plant development and responses to environmental stresses^{1–3}. The levels of ABA in plants are dynamically controlled through tightly regulated biosynthesis and metabolism^{3,4}. ABA biosynthesis involves multiple enzymatic steps, with the cleavage of carotenoids by 9-cis-epoxycarotenoid dioxygenase (NCED), abscisic acid deficient 2

(ABA2), and abscisic aldehyde oxidase (AAO3)^{3,4}. Under abiotic stress conditions, such as drought and high salinity, specific signaling pathways are activated, leading to increased ABA accumulation^{5,6}.

The ABA signaling pathway is initiated by binding of ABA to its receptors, which include PYRABACTIN RESISTANCE1 (PYR1), PYRABACTIN-LIKE (PYL), and REGULATORY COMPONENTS OF ABA

¹Key Laboratory of Plant Cell and Chromosome Engineering, Institute of Genetics and Developmental Biology, Chinese Academy of Sciences, Beijing, China.

²University of Chinese Academy of Sciences, Beijing, China. ³School of Life Sciences and Biotechnology, Shanghai Jiao Tong University, Shanghai, China. ⁴Key Laboratory of Plant Genomics, Institute of Genetics and Developmental Biology, Chinese Academy of Sciences, Beijing, China. ⁵Hunan University, Changsha, China. ⁶John Innes Centre, Norwich Research Park, Norwich, UK. ⁷Center for Excellence in Molecular Plant Sciences, Chinese Academy of Sciences, Shanghai, China. ⁸RNA Biology and Molecular Physiology, Faculty of Biology, Bielefeld University, Bielefeld, Germany. ⁹CAS-JIC Centre of Excellence for Plant and Microbial Science (CEPAMS), Institute of Genetics and Developmental Biology, CAS, Beijing, China. ¹⁰These authors contributed equally: Jing Zhang, Wenna Shao, Yongxin Xu. ✉ e-mail: yuxiang2021@sjtu.edu.cn; jxiao@genetics.ac.cn

RECEPTORS (RCAR)^{7,8}. These receptors interact with PROTEIN PHOSPHATASE 2Cs (PP2Cs), forming a complex that inhibits the phosphatase activity of PP2Cs, thereby activating SNF1-RELATED PROTEIN KINASE 2s (SnRK2s)⁹. The activated SnRK2s then stimulate ABRE-binding protein/ABRE-binding factors (AREB/ABF), leading to enhanced transcription of ABA-responsive genes¹⁰. In addition to facilitating downstream transcriptional regulation, research has indicated that ABA also suppresses global mRNA translation¹¹. Notably, the SUPPRESSOR OF THE ABAR OVEREXPRESSION 1 (SOAR1) protein, a member of the pentatricopeptide repeat (PPR) family, inhibits the translation of *ABA INSENSITIVE 5 (ABI5)* by binding to its mRNA, thereby negatively regulating ABA signaling¹². Further research is essential to unravel the complex interplay between ABA signaling and translational regulation, enhancing the understanding of how ABA governs plant responses to environmental cues.

Translation is a dynamic process that involves interactions among mRNAs, transfer RNAs, and the ribosomal machinery, regulated by both cis- and trans-acting factors while integrating various internal and external signals^{13,14}. The ribosome serves as a complex molecular machine essential for catalyzing protein synthesis with speed and accuracy¹⁵. In plants, the cytoplasmic ribosome consists of two subunits: the 40S subunit, which decodes the mRNA, and the 60S subunit, responsible for the peptidyl transferase reaction¹⁶. The 40S subunit contains 18S rRNA and 33 ribosomal proteins, while the 60S subunit includes 5S, 5.8S, and 28S rRNAs, along with 47 ribosomal proteins^{17,18}.

Highly translated mRNAs are typically associated with more ribosomes (polysomes) than poorly translated mRNAs¹⁹. Polysome profiling is a common technique for analyzing the translational status of genes, where ribosomal occupancy (the percentage of transcripts associated with ribosomes) and ribosomal density (the number of ribosomes per mRNA) reflect translational efficiency²⁰. However, this method has limitations in resolution and accuracy²¹. To better understand translational regulation, it is crucial to measure the dynamic positional information and abundance of translating ribosomes on individual transcripts²². Ribosome profiling, which involves deep sequencing of the ribosome-protected mRNA fragments, was developed to map the positions of translating ribosomes on transcripts²¹. This technique has been instrumental in elucidating the molecular basis of translational regulation in photomorphogenesis²². Subsequent improvements in footprint precision and data quality by employing RNase T1 have enhanced its applicability^{23,24}, providing a rich foundation for studying translation regulation in detail²⁵.

Translational control plays a vital role in plant development^{26,27} and stress responses^{28,29}. In rice, the RNA-binding protein MAO HUZ19 (MHZ9), which contains a glycine-tyrosine-phenylalanine (GYF) domain, responds to ethylene signals by binding to the 3' untranslated region (UTR) of EIN3 BINDING F-BOX (EBF) mRNA. This interaction leads to translational inhibition and significantly contributes to downstream ethylene signaling pathways²⁸.

RNA-binding proteins (RBPs) are crucial for post-transcriptional regulation of RNAs, influencing various aspects of RNA metabolism, including splicing, stability, localization, and translation³⁰. They interact dynamically with RNA partners, participating in nearly all stages of RNA processing and function. The roles of many RBPs in plant development and stress responses have been documented³¹. Among these, glycine-rich RNA-binding proteins (GRPs) are particularly abundant and linked to abiotic stress responses in plants³². The GRP family consists of eight members, whose mRNA level can be induced by abiotic stresses. Under drought stress, the expression of *GRP2*, *GRP4*, and *GRP7* decreases, while *GRP3*, *GRP4*, *GRP6*, and *GRP7* show reduced expression under high salinity³³. *GRP7*, a well-studied member, shares high sequence similarity with GRP8 and exhibits functional redundancy with it³⁴. The *grp7-1 8i* mutant, which has an RNAi construct against AtGRP8 and expresses GRP8 at levels comparable to Col-0

plants, displays hypersensitivity to abscisic acid (ABA), and GRP7 protein levels significantly decline upon ABA treatment³⁵.

GRP7 features an N-terminal RNA recognition motif and a C-terminal glycine-rich domain that enables nucleocytoplasmic shuttling. It facilitates mRNA export from the nucleus to the cytoplasm during cold stress³⁶ and regulates flowering time by influencing RNA processing³⁷. GRP7 also affects RNA stability, impacting the circadian oscillation of the target mRNA *LHCBI.38*. Mutations in GRP7 have been shown to alter the content of both small RNAs (sRNA) and long non-coding RNAs (lncRNA) in apoplastic wash fluid (AWF), suggesting its involvement in the secretion and/or stabilization of exRNAs³⁹. Notably, GRP7 participates in innate immunity by translation regulation, interacting with eukaryotic translation initiation factors (eIF4A1, eIF4A2, eIF4E), and ribosomal protein uS11z⁴⁰. At elevated temperatures, GRP7 forms condensates in the cytoplasm through liquid-liquid phase separation, inhibiting the translation of *GRP7* and *HSP70-I*⁴¹. However, the extent of GRP7's role in global mRNA translation efficiency remains unclear.

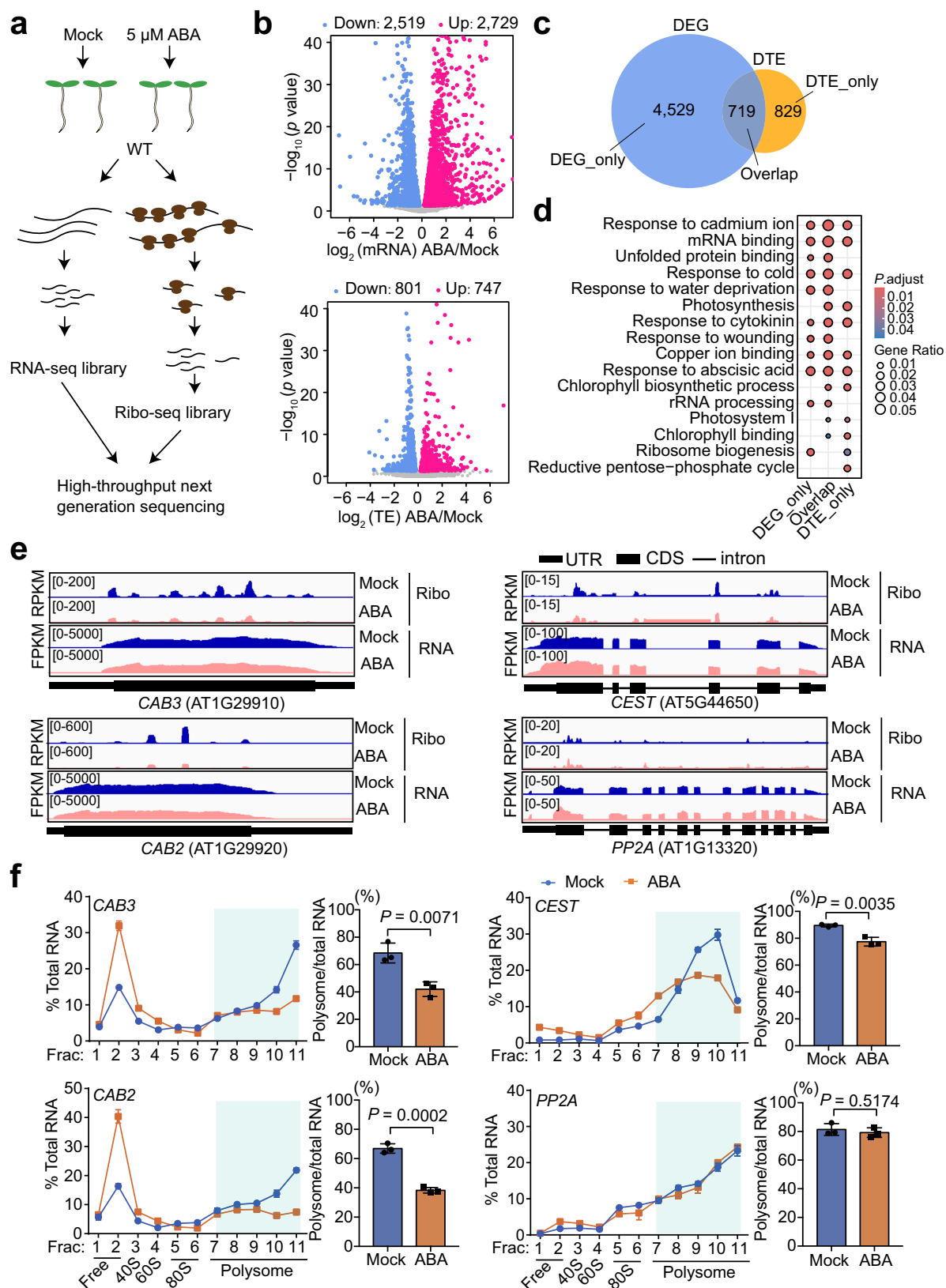
In this study, we observed that ABA treatment not only induced significant mRNA level changes but also caused a multitude of alterations in translation efficiency in *Arabidopsis thaliana*, as detected by Ribo-seq and RNA-seq analyses. Furthermore, ABA treatment leads to a reduction in the protein levels of GRP7&8 through its core signaling factors. GRP7&8 can associate with ribosomes to influence mRNA translation efficiency and plays a crucial role in ABA signal-mediated translational regulation by directly binding to its target mRNAs. Additionally, the regulation of mRNA translation efficiency under drought stress is partially dependent on the ABA-GRP7&8 pathway.

Results

Differential regulation of gene expression and translation efficiency in response to ABA treatment

Plant exhibits rapid adjustments in gene expression at both transcriptional and translational levels in response to environmental stress, with the hormone ABA playing a pivotal role^{42,43}. By conducting RNA-seq and Ribo-seq analyses on three-day-old Col-0 seedling subjected to 5 μ M ABA or mock treatment for 4 h, we explored the genes with differential mRNA and translation levels (Fig. 1a). As expected, strong correlation existed between steady-status RNA levels and translation levels within the same sample (Supplementary Fig. 1a). TE is calculated using normalized Ribo-seq reads divided by RNA-seq reads (see "Methods" for details).

Under ABA treatment, we identified 5248 differentially expressed genes (DEGs) and 1548 genes exhibiting differential translation efficiency (DTE) (Fig. 1b and Supplementary Data 1, 2). Among these, 719 genes showed ABA-induced changes at both the mRNA and translational levels (Overlap), while 4529 genes were altered only at the mRNA level (DEG_only) and 829 genes only at the translational level (DTE_only) (Fig. 1c). Genes involved in the response to abscisic acid, cytokinin, cold, and mRNA binding exhibited changes at both levels (Fig. 1d). In contrast, genes related to ribosome biogenesis were primarily regulated at the mRNA level, whereas those involved in photosynthesis and chlorophyll biosynthesis were predominantly affected at the translational level (Fig. 1d). Notably, genes that were upregulated in both mRNA and translation efficiency were associated with responses to abiotic stresses (Supplementary Fig. 1b). Conversely, genes with downregulated translation efficiency were enriched in photosynthesis and chlorophyll biosynthetic process. Specifically, genes related to photosynthesis and chloroplast biogenesis, such as *Chlorophyll A/B binding proteins 2 and 3 (CAB2, At1g29920; CAB3, At1g29910)*^{38,44} and *Chloroplast Protein-Enhancing Stress Tolerance (CEST, At5g44650)*⁴⁵, underscore the critical role of translational regulation in the ABA response (Fig. 1e). In contrast, *PROTEIN PHOSPHATASE 2A SUBUNIT A3 (PP2A, At1g13320)* served as a negative control,



showing no changes in translation efficiency or RNA levels in response to ABA (Fig. 1e).

To further evaluate the translation efficiency of individual genes exhibiting differential TE under ABA treatment from Ribo-seq data, we measured mRNA levels in entire fractions of polysome profiling using RT-qPCR. The results were expressed as a percentage of the

total RNA in each fraction. To quantify TE, we calculated the proportion of polysome-bound RNA (fractions 7–11) relative to the total RNA. This analysis confirmed that the TE of the photosynthesis genes *CAB2*, *CAB3*, and *CEST* decreased upon ABA treatment in Col-0, while the negative control gene *PP2A* showed no significant changes (Fig. 1f).

Fig. 1 | ABA globally modulates translation efficiency. **a** Schematic representation of RNA-seq and Ribo-seq using Col-0 seedlings with mock or 5 μ M ABA treatment for 4 h. **b** Volcano plots displaying significant changes in mRNA level (upper panel) and translation efficiency (bottom panel) in Col-0 seedlings treated with ABA, compared to mock. The *P*.adjust value refers to the Benjamini–Hochberg procedure adjusted *P* values of two-sided Wald test. **c** Venn diagram displaying the overlap between differentially expressed genes (DEG, mRNA level) and genes with altered translation efficiency (DTE) under ABA treatment. **d** Enriched GO terms for genes in (c), with altered only at the mRNA level (DEG_only), only at the translational efficiency level (TE_only), and at both levels (Overlap) under ABA treatment. The size of dots indicates gene ratio, which refers to the fraction of genes associated with a given GO term out of all the genes that were identified as differentially expressed. The color representing the *P*.adjust value, which refers to the Benjamini–Hochberg procedure adjusted *P*-values of the One sided Hypergeometric test. **e** IGV

showcasing the distribution of RNA-seq and Ribo-seq reads across *CAB2*, *CAB3*, *CEST* genes with altered TE under mock and ABA treatment, *PP2A* serves as negative control with no change upon ABA treatment. Y axis shows fragments/reads per kilobase per million mapped reads (FPKM/RPKM). The gene models are depicted with lines representing introns and rectangles of varying thickness indicating the CDS and UTR, respectively. **f** Relative mRNA levels of *CAB2*, *CAB3*, *CEST* and *PP2A* (negative control) across different fractions of polysome profiling in Col-0 seedlings upon mock and ABA treatment (left). Data are the mean \pm SD of three technical replicates from one representative polysome profiling experiment. To quantify the translation efficiency, the proportion of polysome-bound RNA (fractions 7–11, light green shade) relative to the total RNA under mock and ABA treatment were displayed in bar graph (right). Data are mean \pm SD from three biological replicates of independent polysome profiling experiments. *P* value was calculated by two-sided Student's *t* test. Source data are provided as a Source Data file.

In summary, ABA treatment in Col-0 seedlings caused significant changes in gene expression, revealing the role of translational regulation alongside transcriptional regulation.

ABA signaling pathway components regulate global mRNA translation efficiency

We examined the impact of ABA signaling pathway factors on mRNA translation efficiency by focusing on the ABA receptor mutant *pyr1-pyl1/2/4*^{46,47}, the negative regulator phosphatase triple mutant *abi1-2/abi2-1/habi1-1* (*pp2c 3 m*)^{48,49}, and the key kinase mutant *snrk2.2/2.3/2.6*^{50,51}. We performed polysome profiling, which separates mRNA bound to different numbers of ribosomes using a sucrose gradient in ultracentrifugation²⁰. This analysis evaluated the global translation activity in Col-0 and the ABA signaling mutants, comparing mock treatment to 5 μ M ABA treatment for 4 h of three-day-old seedlings (Fig. 2a–d). As previously reported¹¹, ABA treatment significantly reduces the polysome/monosome ratio in Col-0 compared to mock treatment, validating our polysome profiling approach (Fig. 2a).

In our polysome profiling analysis, the *pyr1pyl1/2/4* mutant, which is less sensitive to ABA⁴⁷, showed no significant changes in the polysome/monosome ratio compared to Col-0 under mock condition (Supplementary Fig. 2). The *pp2c 3 m* mutant, known to be hypersensitive to ABA during seed germination and root growth⁴⁹, displayed a reduced polysome/monosome ratio compared to Col-0 under mock condition, similar to Col-0 treated with ABA (Fig. 2a, Supplementary Fig. 2). In contrast, the *snrk2.2/2.3/2.6* mutant, which is almost completely insensitive to ABA and exhibits rapid water loss⁵¹, also demonstrated a reduced polysome/monosome ratio under mock condition (Supplementary Fig. 2). This water-sensitive state likely contributed to its decreased translation efficiency, as drought is known to inhibit mRNA translation⁵².

Notably, in response to ABA treatment, the polysome/monosome ratios in the *pyr1pyl1/2/4*, *pp2c 3 m*, and *snrk2.2/2.3/2.6* mutants showed no significant changes compared to mock conditions in contrast to Col-0 (Fig. 2a–d), further confirming that core components of ABA signaling are essential for regulating the polysome profiles. To assess the role of ABA signaling components in regulating TE changes at specific genes, we quantified the down-regulation of the photosynthesis gene *CEST* and the abiotic stress response gene *FRUCTOSE-BISPHOSPHATE ALDOLASE 2* (*FBA2*, At4g38970)⁵³ upon ABA treatment in different mutants using ribosome fractionation and qPCR. While Col-0 showed reduced TE for *CEST* and *FBA2* in response to ABA, the *pyr1pyl1/2/4*, *pp2c 3 m*, and *snrk2.2/2.3/2.6* mutants did not exhibit significant changes (Fig. 2e). The negative control *PP2A* showed no alterations in TE under ABA treatment compared to mock conditions in all tested plants (Fig. 2e).

Thus, ABA-mediated regulation of mRNA translation efficiency is accompanied by signal transduction from receptors to core signaling components, including phosphatases and kinases.

GRP7&8 is involved in ABA-mediated translational efficiency regulation

Given the changes in polysome profiling mediated by ABA signaling, we sought to identify factors associated with ribosomes that are regulated by the ABA signaling pathway. Immunoprecipitation followed by mass spectrometry (IP-MS) was used to identify these ribosome-associated factors. Using anti-Flag, we conducted IP on 3-days-old seedlings of *pACTIN2::Flag-eL18y* (see material for details), a component of the large ribosomal subunit¹⁷ (Fig. 3a, b), with Col-0 as a negative control. Co-immunoprecipitated proteins identified in both replicates from *pACTIN2::Flag-eL18y* but absent in Col-0 were considered associated factors with eL18y (Supplementary Data 3).

In addition to ribosomal subunits, mRNA binding proteins were enriched, including eight non-ribosomal RNA-binding proteins (RBPs) (Fig. 3c). Notably, GRP7 and *COLD SHOCK PROTEIN 2* (*CSP2*, At4g38680) are RBPs that respond to ABA and exhibit altered sensitivity when mutated^{54,55}. Furthermore, a suite of mRNAs previously reported GRP7 mRNA targets from individual nucleotide resolution Crosslinking and Immunoprecipitation Sequencing (iCLIP-seq) data⁵⁶ significantly overlapped with genes showing upregulated or downregulated translation efficiency in response to ABA treatment in this study (Fig. 3d). Under ABA treatment, iCLIP-seq identified GRP7 targets with downregulated translation efficiency were primarily enriched in pathways related to photosynthesis, while targets with upregulated translation efficiency were mainly involved in water transport and channel activity (Fig. 3e). Collectively, these findings suggest that GRP7 may act as a key regulator in ABA-mediated translation regulation.

GRP8 closely resembles GRP7, displaying high sequence similarity and functional redundancy in regulating alternative splicing³⁴ and flowering⁵⁷. To further elucidate their roles in ABA-regulated plant development and potential involvement in mRNA TE regulation, we generated a *grp7grp8* double mutant by editing the *GRP8* gene in the *grp7-1* background (Supplementary Fig. 3a). A single nucleotide insertion (A or G) in the first exon of *GRP8* resulted in an altered reading frame with a stop codon at either the 8th or 36th amino acid position (Supplementary Fig. 3a). The seed germination of the *grp7-1* mutant is hypersensitive to ABA⁵⁵. Notably, both *grp7grp8^{CR}-A/G* mutant lines exhibited significantly higher ABA sensitivity than either the *grp7-1* or *grp8^{CR}-A/G* single mutants (Supplementary Fig. 3b), indicating the redundant functions of GRP7 and GRP8 in ABA-mediated inhibition of cotyledon greening.

We then performed the polysome profiling of Col-0 and *grp7grp8^{CR}-A/G* mutant lines under both mock and ABA treatments for 4 h. Notably, both *grp7grp8^{CR}-A/G* lines exhibited a reduced polysome/monosome ratio compared to Col-0 at mock condition (Fig. 3f, g), similar to the effect observed in Col-0 under ABA treatment (Supplementary Fig. 3c-top panel). When examining the polysome profiles

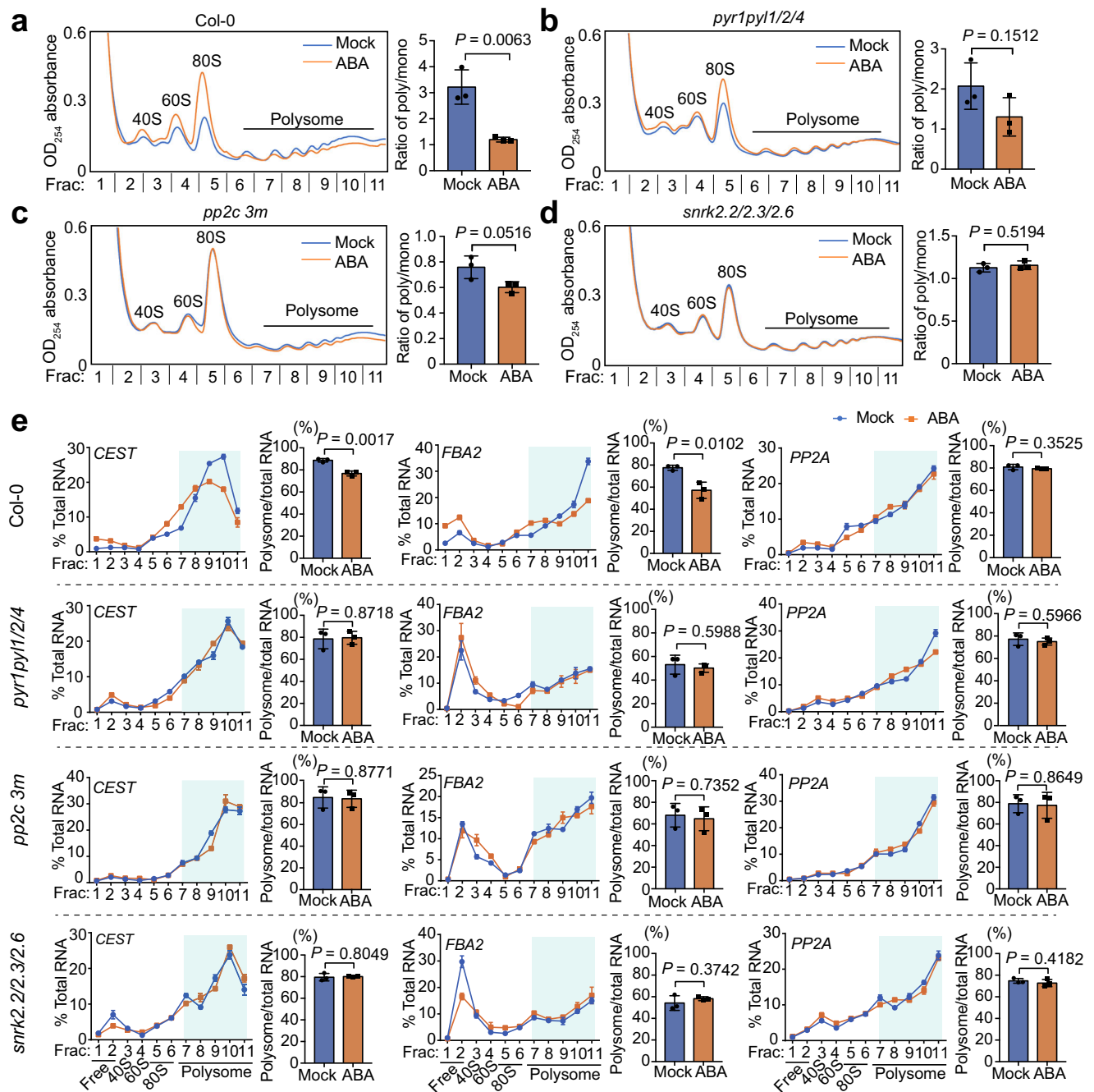


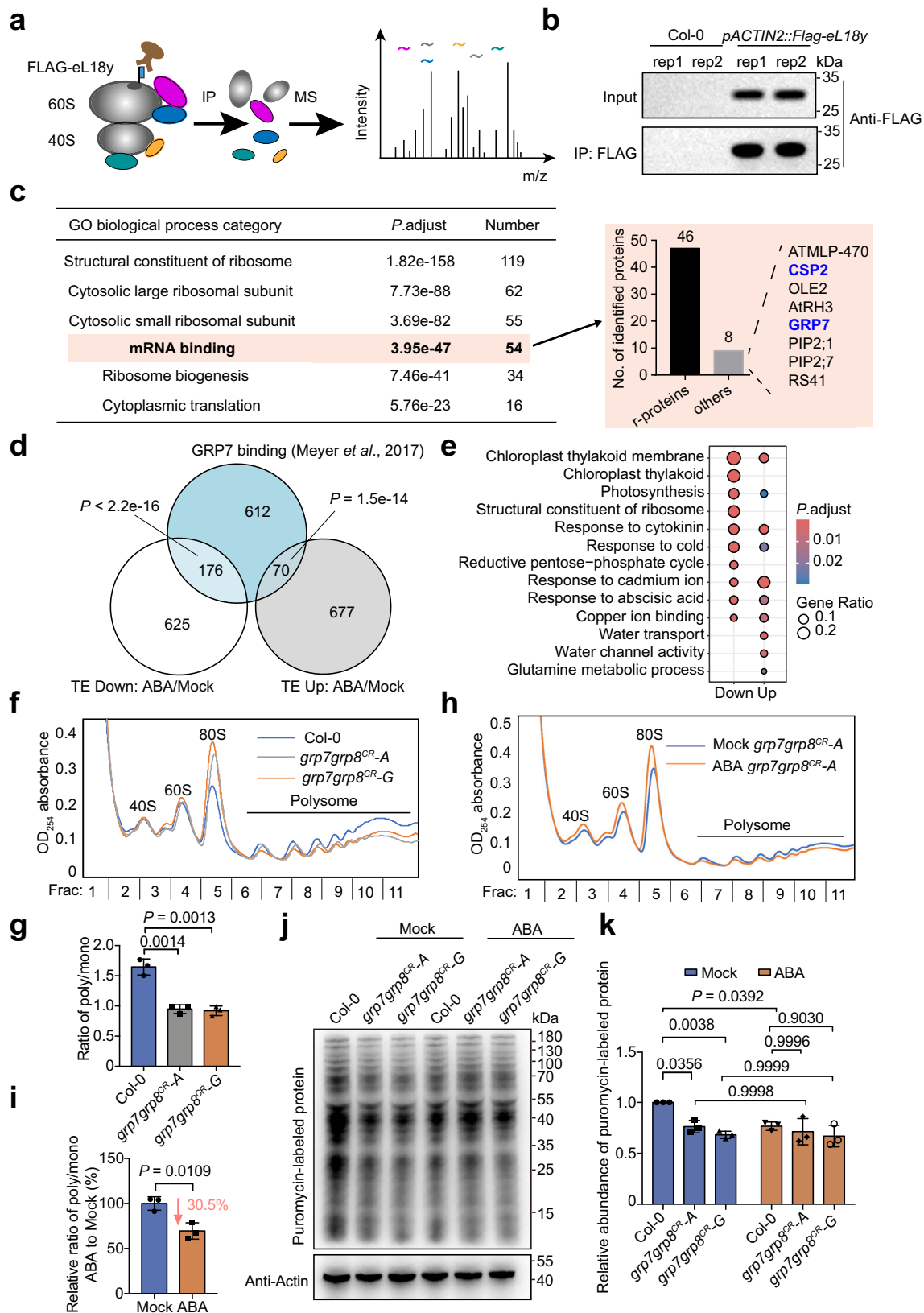
Fig. 2 | ABA affects translation efficiency through its signaling pathway factors.

a–d Representative absorbance plot in polysome profiling of Col-0 (**a**), *pyr1/pyl1/2/4* (**b**), *pp2c 3m* (**c**) and *snrk2.2/2.3/2.6* (**d**) with mock and ABA treatment for 4 h. Ribosomes were isolated by sucrose density gradient centrifugation using a 10–50% gradient, yielding fractionation 1–11. Comparison of quantified polysome/monosome (poly/mono) ratios between mock and ABA treatment on the right. The values are means \pm S.D. of three biological replicates. P value was calculated by two-sided Student's t test. **e** Relative mRNA levels of *CEST*, *FBA2*, and *PP2A* (negative control) across different fractions of polysome profiling in Col-0, *pyr1/pyl1/2/4*, *pp2c 3m* and

snrk2.2/2.3/2.6 seedlings upon mock and ABA treatment for 4 h (left). Data are the mean \pm S.D. of three technical replicates from one representative polysome profiling experiment. To quantify the translation efficiency, the proportion of polysome-bound RNA (fractions 7–11, light green shade) relative to the total RNA under mock and ABA treatment were displayed in bar-graph (right). Data are mean \pm S.D. from three biological replicates of independent polysome profiling experiments. P value was calculated by two-sided Student's t test. Source data are provided as a Source Data file.

during ABA treatment, both *grp7grp8^{CR}-A/G* lines showed lesser reduction in the polysome/monosome ratio, but ABA treatment still resulted in decreased ribosome loading efficiency in both mutant lines (Fig. 3h, i and Supplementary Fig. 3c–lower panel). This indicates that GRP7 and GRP8 partially mediate the effect of ABA on the global decline in mRNA translation efficiency. Additionally, the surface sensing of translation (SUnSET) assay (see "Methods"s for

details) demonstrated that, under mock conditions, protein synthesis efficiency in *grp7grp8^{CR}-A* and *grp7grp8^{CR}-G* was lower compared to Col-0. Under ABA treatment, Col-0 displayed a decrease in protein synthesis efficiency, while almost no decrease was detected in the *grp7grp8^{CR}-A* and *grp7grp8^{CR}-G* lines (Fig. 3j, k). These results suggest that GRP7&8 plays a role in the regulation of translation in response to ABA.



ABA signaling regulates GRP7&8 level to participate in translation regulation

To further validate the association of GRP7&8 with the ribosomal machinery in the cytoplasm, we separated different mRNA-bound ribosome fractions using a sucrose gradient through ultracentrifugation of lysates from three-day-old *pACTIN2::Flag-eL18y* seedling treated

with mock or 5 μ M ABA for 4 h. Following this, we performed immunoblotting with various antibodies (Fig. 4a). We generated a GRP7 antibody based on a previous publication³⁷, which detect both GRP7 (16.9 kDa) and GRP8 (16.6 kDa) in Col-0, given their marginal size difference (Supplementary Fig. 4a). The Flag antibody was employed to detect Flag-eL18y, a component of the large ribosomal subunit,

Fig. 3 | GRP7 is involved in ABA-mediated translation efficiency regulation. **a** Schematic illustrating the detection of ribosome interacting proteins using IP-MS. **b** Immunoprecipitation of eL18y protein was detected by western blot with anti-FLAG. The immunoprecipitation experiment had two biological replicates. **c** GO enrichment of proteins associated with FLAG-eL18y by IP-MS, and the RNA binding protein was highlight with light orange shade. CSP2 and GRP7 reported to response to ABA treatment were marked in blue. The *P*-adjust value refers to the Benjamini–Hochberg procedure adjusted *P* values of one-sided Hypergeometric test. **d** Overlapping of GRP7-binding genes and genes with altered translation efficiency under ABA treatment for 4 h. One-sided Hypergeometric tests were used to calculate the *P* values for the enrichment of genes. **e** GO enrichment of GRP7 target mRNAs that with altered translation efficiency under ABA treatment. *P*-adjust value refers to the Benjamini–Hochberg procedure adjusted *P* values of one-sided Hypergeometric test. **f, g** Representative polysome profiling absorbance plot (**f**) and quantified polysome/monosome (poly/mono) ratios (**g**) of Col-0 and

grp7grp8^{CR}-A/G lines under mock were shown. The values are means \pm S.D. (*n* = 3 biological replicates). *P* value was calculated by two-sided Student's *t* test. **h, i** Representative polysome profiling absorbance plot (**h**) and quantified relative polysome/monosome ratios of *grp7grp8^{CR}-A* under ABA treatment for 4 h compared to mock (**i**) were shown. The pink arrow indicates the decrease in the polysome/monosome ratio under ABA treatment, and the pink number represents the percentage of decrease. The values are means \pm S.D. (*n* = 3 biological replicates). *P* value was calculated by two-sided Student's *t* test. **j** SUNSET assay detecting new synthesized proteins upon mock and ABA treatment for 4 h in Col-0 and *grp7grp8^{CR}-A/G* lines, shown was one representative result out of three biological replicates (see "Methods" for details). **k** Quantification of the relative abundance of puromycin-labeled protein in (**j**) was performed using actin as the loading control. The values are means \pm SD (*n* = 3 biological replicates). *P* value was calculated by Two-way ANOVA. Source data are provided as a Source Data file.

while eS6z marked the small ribosomal subunit¹⁷. GLYCERALDEHYDE-3-PHOSPHATE DEHYDROGENASE C SUBUNIT (GAPDH, At3g04120) served as a control protein not associated with ribosomes⁵⁸.

As expected, Flag-eL18y was detected in the 60S large subunit, 80S monosome and polysome fractions, while eS6z was primarily found in the 40S small subunit, 80S monosome and polysome fractions under both mock and ABA treatment conditions (Fig. 4a), validating our procedure. GRP7&8 co-fractionated with the 40S and 60S ribosomal subunits, monosome, and polysome fractions (Fig. 4a), suggesting their active participation in the translation process. To rule out the possibility of non-ribosomal complexes co-fractionating, we treated the lysates with EDTA to disassemble 80S monosomes into 40S and 60S ribosomal subunits, which resulted in the depletion of GRP7&8 from the monosome and polysome fractions (Supplementary Fig. 4b–left). Additionally, treatment with RNase A, which promotes the accumulation of 80S monosomes, led to a substantial reduction in GRP7&8 levels within polysome fractions (Supplementary Fig. 4b–right). These findings robustly support the association between GRP7&8 and actively translating mature ribosomes.

Notably, under ABA treatment, the amount of GRP7&8 co-fractionating with polysome appeared reduced compared to mock conditions (Fig. 4a). Furthermore, a Co-IP assay confirmed that GRP7&8 interact with eL18y under both mock and ABA treatments (Fig. 4b). Importantly, this interaction was unaffected by ABA treatment when normalizing the GRP7 or GRP8 protein levels from IP sample to input samples (Fig. 4c). These results suggest that while ABA treatment does not influence the interaction between GRP7&8 and ribosomes, it likely affects their association with active translation polysomes.

We further examined the impact of ABA treatment on the expression of GRP7 and GRP8. RNA-seq data, confirmed by qPCR, revealed that the transcript levels of GRP7 and GRP8 significantly decreased in three-day-old seedling exposed to 5 μ M ABA for 4 h (Fig. 4d), consistent with previous reports⁵⁵. qPCR analysis of entire fractions of polysome profiling also indicated a reduction in the TE of both mRNAs under ABA treatment (Fig. 4e), suggesting that their protein levels are likely diminished. Ribo-seq data revealed a notable decrease in the translational levels of GRP7 and GRP8 in Col-0 following ABA treatment (Supplementary Fig. 4c). Indeed, protein levels of GRP7 and GRP8 were significantly reduced in three-day-old seedlings treated with 5 μ M ABA compared to mock (Fig. 4f, g). This reduction did not appear to be related to protein stability, as no differences in GRP7 and GRP8 levels was observed between mock and ABA treatments with the prior addition of cycloheximide (CHX) (Supplementary Fig. 4d), which inhibits new protein synthesis⁵⁹. Importantly, the decrease in GRP7 and GRP8 protein levels upon ABA treatment was abolished in core ABA signaling mutants such as *pyr1-pyl1/2/4*, *pp2c 3m* and *snrk2.2/2.3/2.6* (Fig. 4f, g). Thus, ABA signaling

activation likely reduces GRP7 and GRP8 levels by reducing RNA levels and translation efficiency at the three-day-old seedling stage.

To genetically confirm the role of GRP7/8 in the ABA signaling pathway, we crossed *snrk2.2/2.3/2.6* with *grp7grp8^{CR}-G* to create the homozygous quintuple mutant *snrk2.2/2.3/2.6 grp7grp8^{CR}-G* (*5m*) (Supplementary Fig. 4e). We assessed the germination rates of Col-0, *snrk2.2/2.3/2.6*, *grp7grp8^{CR}-G*, and *5m* on 1/2 MS medium with 0 μ M, 1 μ M, and 50 μ M ABA, around 48 h post-stratification. As reported^{35,51}, *snrk2.2/2.3/2.6* was resistant while *grp7grp8^{CR}-G* was sensitive to ABA compared to Col-0 (Fig. 4h, i, Supplementary Fig. 4f, g). Under low ABA concentration (1 μ M), the sensitivity of *5m* matched that of *snrk2.2/2.3/2.6* (Supplementary Fig. 4f, g). However, at high ABA concentration (50 μ M), *5m* was more sensitive than *snrk2.2/2.3/2.6* (Fig. 4h, i), indicating GRP7&8's role in mediating morphological responses to elevated ABA levels.

GRP7&8 mediates ABA signaling-regulated mRNA translation efficiency

To assess the role of GRP7&8 in translation efficiency regulation, we performed Ribo-seq and RNA-seq on *grp7grp8^{CR}-A* with mock and ABA treatment for 4 h. Firstly, quality assessment using principal component analysis revealed a high degree of reproducibility among three biological replicates of RNA-seq and Ribo-seq data (Supplementary Fig. 5a). Next, we analyzed the features of the ribosome footprint revealed by Ribo-seq reads. We found that the most abundant Ribo-seq read lengths were 27 and 28 nt (Supplementary Fig. 5b), and the Ribo-seq reads mapped to 3' UTR were significantly decreased compared to RNA-seq reads (Supplementary Fig. 5c). Notably, the distribution of Ribo-seq 5' end counts across CDS displayed 3-nt periodicity pattern and Ribo-seq 5' end counts were enriched at 15–18 nt upstream of start codon and stop codon (Supplementary Fig. 5d–g). Notably, second peaks were found around start codon, which have been consistently observed in many ribosome profiling datasets due to ligate sequence preference^{60,61}. Overall, these features indicate the high quality of these Ribo-seq profiling data. As expected, the abundance of RNA-seq read mapped to each gene were strongly correlated with the abundance of Ribo-seq reads within the same sample (Supplementary Fig. 6).

In *grp7grp8^{CR}-A*, the mRNA abundance levels of 759 and 1087 genes were significantly changed compared to Col-0 under mock and ABA treatment, respectively (Fig. 5a and Supplementary Data 4, 8). However, at the translational level, 2062 genes and 2077 genes displayed altered TE in the *grp7grp8^{CR}-A* under normal conditions and ABA treatment, respectively (Fig. 5b, Supplementary Data 6, 9). These results indicate that GRP7&8 affects more genes through translational regulation than at the mRNA level. Under mock condition, 250 genes exhibited changes at both mRNA and translational level in *grp7grp8^{CR}-A* compared to Col-0. Additionally, 509 genes displayed altered mRNA level but maintained unchanged TE, while 1,812 genes changed TE while their mRNA level remained constant (Fig. 5c). Remarkably, genes

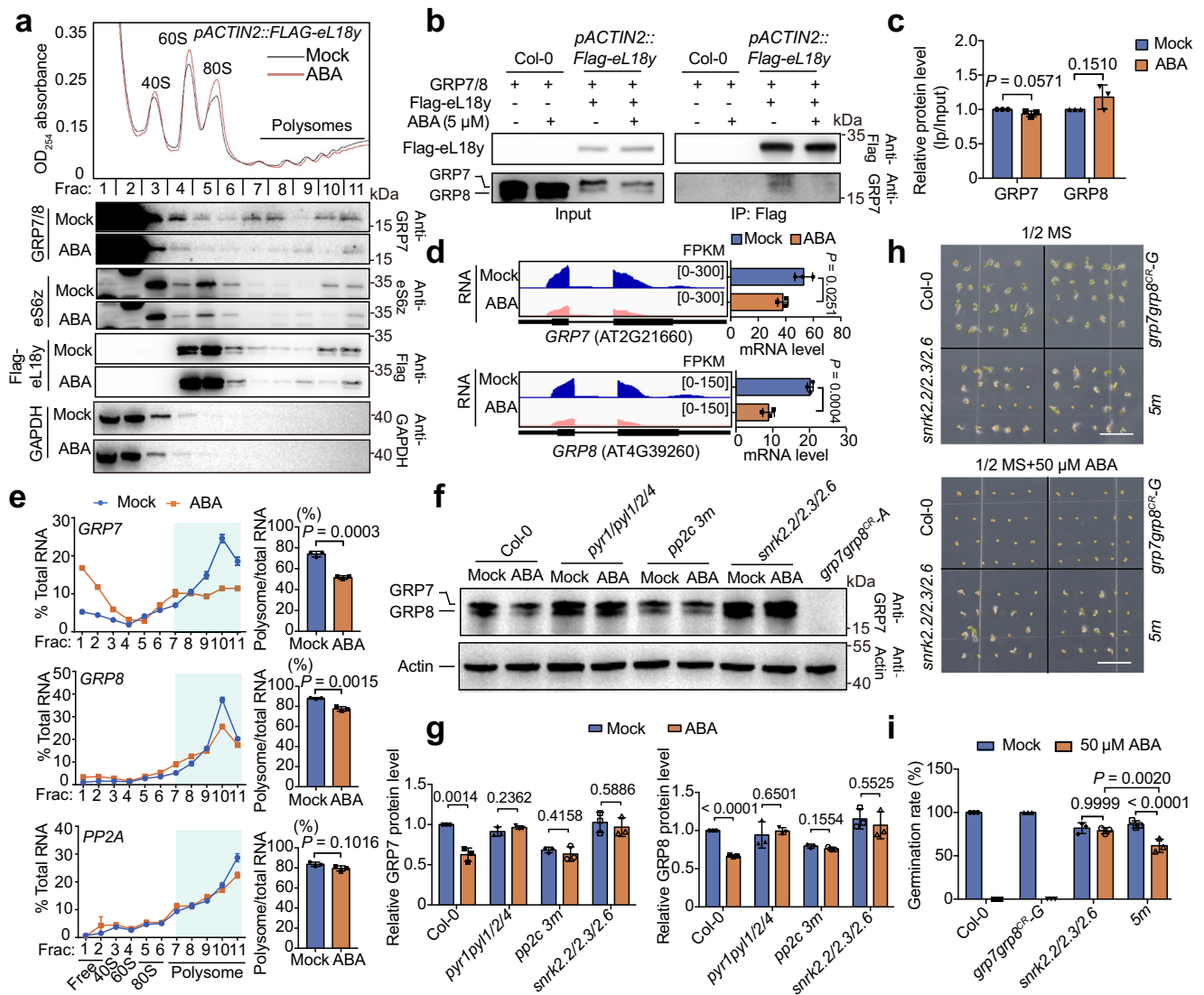


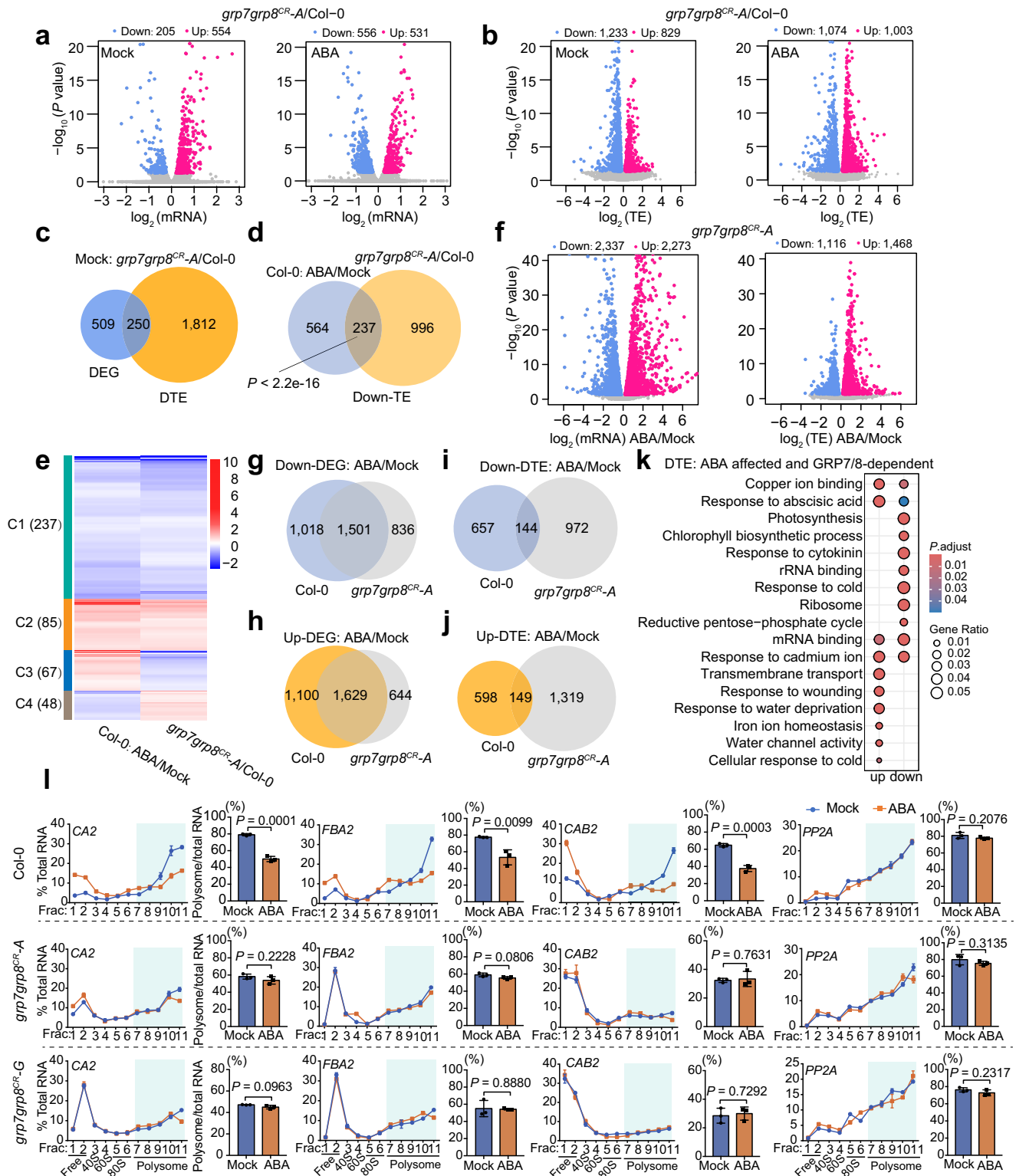
Fig. 4 | ABA signal reduces GRP7 protein to participate in translation regulation. **a** Polysome profiles of *pACTIN2::FLAG-eL18y* (top) and western blots of GRP7, eS6z, FLAG-eL18y and GAPDH (negative control) from corresponding fractions (bottom) with mock and ABA treatment for 4 h. Experiment repeated three times with similar results. **b** Co-IP result of GRP7&8 and eL18y in *pACTIN2::FLAG-eL18y* and Col-0 under mock and ABA treatment for 4 h. **c** Quantification of GRP7 and GRP8 signals in (b). The values are means \pm S.D. (n = 3 biological replicates). **d** GRP7 and GRP8 expression level under mock and ABA treatment determined by RNA-seq (left) and RT-qPCR (right). Y-axis in IGV: FPKM. RNA from 3-day-old Col-0 seedlings treated with mock or 5 μ M ABA for 4 h was used for RT-qPCR, with *PP2A* as the reference. The values are means \pm S.D. (n = 3 technical replicates). **e** Relative mRNA levels of *GRP7*, *GRP8*, and *PP2A* (negative control) across different fractions in Col-0 upon mock and ABA treatment (left). Data are the mean \pm S.D. of three technical

replicates from one representative polysome profiling. Polysome-bound RNA (light green) vs. total RNA in bar graph (right). Data are mean \pm S.D. (n = 3 biological replicates). **f** Detection of GRP7 and GRP8 protein levels in Col-0, *pyr1pyl1/2/4*, *pp2c 3m* and *snrk2.2/2.3/2.6* upon mock and ABA treatment for 4 h using an anti-GRP7 antibody. **g** Quantification of GRP7 and GRP8 signals in (f) using actin as the loading control. The values are means \pm S.D. (n = 3 biological replicates). **h, i** Germination rate of Col-0, *grp7grp8^{CR-G}*, *snrk2.2/2.3/2.6*, and *snrk2.2/2.3/2.6 grp7grp8^{CR-G}* (5m) seedlings on 1/2 MS medium containing 0 μ M and 50 μ M ABA. Representative photographs (h) of genotypes (each biological replicate with 20 seedlings; Scale bars, 5 mm) were shown. The comparison of germination rate of genotypes were shown in bar plot (i), data are means \pm S.D. (n = 3 biological replicates). *P* value in (c–e, g) were calculated by two-sided Student's *t* test. *P* value in (i) were calculated by Two-way ANOVA. Source data are provided as a Source Data file.

exhibiting ABA-repressed TE in Col-0 significantly overlapped with genes displaying reduced TE in *grp7grp8^{CR-G}* compared to Col-0 under normal condition. (Fig. 5d). Moreover, the heatmap of genes with altered TE in both Col-0 under ABA treatment and in *grp7grp8^{CR-G}* under mock conditions revealed that the majority of genes (73.68%) exhibited similar patterns of TE change in ABA treatment and the *grp7grp8^{CR-G}* mutation. Among them, most genes showed a significant down-regulation in TE, while a subset of genes exhibited up-regulation in TE (Fig. 5e).

To further explore the effect of GRP7&8 on mediating ABA-triggered mRNA and translation efficiency level changes, we

performed a comprehensive analysis between genes regulated by GRP7&8 and ABA-responsive genes. Under ABA treatment, 4610 DEGs and 2584 genes with DTEs were found in *grp7grp8^{CR-G}* compared to mock, respectively (Fig. 5f and Supplementary Data 5, 7). At mRNA level, we found that, among the 5,248 ABA-induced differentially expressed genes in Col-0, 2,118 (~40.35%) genes changed their responses in *grp7grp8^{CR-G}* mutant plant (Fig. 5g, h and Supplementary Data 1, 5), for detailed data process, see "Methods"). At translational level, among the 1548 genes with ABA-regulated TE alteration in Col-0, 1255 (~81.07%) genes were disrupted in *grp7grp8^{CR-G}* mutant (Fig. 5i, j, Supplementary Data 2, 7). Notably, among those genes with TE



changed in GRP7&8-dependent and ABA-responsive manner, genes with ABA-repressed TE enriched in GO terms related to photosynthesis and chlorophyll biosynthesis, while genes with ABA-promoted TE tend to enrich in response to ABA and response to water deprivation (Fig. 5k). Using polysome profiling followed by RT-qPCR, we further measured the TE of photosynthesis gene *CAB2*, stomatal regulation gene *BETA CARBONIC ANHYDRASE 2* (*CA2*, At5g14740)⁶², and abiotic stress-responsive gene *FBA2* upon ABA treatment in Col-0 and *grp7grp8^{CR}-A/G* mutants, confirming that their down-regulation of TE

after ABA treatment were GRP7&8 dependent (Fig. 5l). This comprehensive analysis establishes GRP7&8 as key mediators of the ABA-regulated translational response.

GRP7&8 mediates translational regulation mainly by directly binding to targets

To explore whether GRP7&8 mediates the translational efficiency regulation of ABA signaling by binding to its target mRNAs, we performed protein-RNA crosslinking and immunoprecipitation (CLIP)-seq

Fig. 5 | ABA-regulated global translational efficiency dependent on GRP7&8. **a, b** Volcano plots showing changes of mRNA level (**a**) and translational efficiency (**b**) in *grp7grp8^{CR}-A* compared to Col-0 seedlings under mock (left) or ABA treatment for 4 h (right). *P*-adjust value refers to the Benjamini-Hochberg procedure adjusted *P* values of two sided Wald test. **c, d** Venn diagram showing overlap of DEG and DTE in *grp7grp8^{CR}-A* under mock condition (**c**), and the overlap of DTE between mock and ABA treatment in Col-0, and DTE between Col-0 and *grp7grp8^{CR}-A* under mock condition (**d**). One-sided Hypergeometric tests were used to calculate the *P* values for the enrichment of genes. **e** The heatmap displays the log₂ fold change of significant differences in translation efficiency (log₂FC_TE) for two comparisons: ABA Col-0 vs Mock Col-0 and Mock *grp7grp8^{CR}-A* vs Mock Col-0. The numbers represent the count of genes within each respective cluster. **f** Volcano plots displaying significant changes of mRNA level (left) and translation efficiency (right) in *grp7grp8^{CR}-A* seedlings between mock and ABA treatment. The *P*-adjust value refers to the Benjamini-Hochberg procedure adjusted *P*-values of two-sided Wald test. **g, h** Venn

diagram illustrating the overlap of genes whose mRNA level suppressed (**g**) and induced (**h**) by ABA treatment in Col-0 and *grp7grp8^{CR}-A*. **i, j** Venn diagram illustrating the number of DTE between Col-0 and *grp7grp8^{CR}-A* whose translational efficiency induced (**i**) and suppressed (**j**) by ABA treatment. **k** GO enrichment of ABA-affected and GRP7/8-dependent DTE. *P*-adjust value refers to the Benjamini-Hochberg procedure adjusted *P*-values of one-sided Hypergeometric test. **l** Relative mRNA levels of *CA2*, *FBA2*, *CAB2* and *PP2A* (negative control) across different fractions of polysome profiling in Col-0 and *grp7grp8^{CR}-A/G* seedlings upon mock and ABA treatment for 4 h (left). Data are the mean ± S.D. of three technical replicates from one representative polysome profiling experiment. The proportion of polysome-bound RNA (fractions 7–11, light green shade) relative to the total RNA were displayed in bar-graph (right). Data are mean ± S.D. (*n* = 3 biological replicates). *P* value was calculated by two-sided Student's *t* test. Source data are provided as a Source Data file.

of GRP7-GFP coupled with GFP-Trap⁶³ (Fig. 6a and Supplementary Fig. 7a, b). RNA-protein complexes were immunoprecipitated with GFP Trap beads and bound RNAs were used for constructing CLIP-seq libraries (Supplementary Fig. 7a, b). Most of the GRP7 targets were enriched at 5' UTRs and exons of protein-coding mRNAs (Fig. 6b, Supplementary Fig. 7c, Supplementary Data 10). Totally, 2468 and 3514 GRP7-binding genes were identified under normal and ABA conditions, respectively. We found that the target mRNAs of GRP7 with mock and ABA treatment significantly overlap with the previously reported GRP7 target mRNAs⁵⁶ (Supplementary Fig. 7d). Overall, 590 (68.76%) out of the 858 known GRP7-binding targets were identified in our CLIP-seq datasets, indicating high-confidence of the identified GRP7 targets. Furthermore, the motifs of GRP7 binding peaks were U/C enriched (Supplementary Fig. 7e), which were consistent with previous report⁵⁶.

Importantly, we found a significant overlap between the target mRNAs of GRP7 under both mock and ABA treatment conditions and the DTE altered by ABA treatment (Fig. 6c). Of the 1548 DTE responsive to ABA, 716 (46.25%) were identified as GRP7-binding targets, which motifs were also U/C enriched (Supplementary Fig. 7e). GO enrichment analysis revealed that genes related to abiotic stress and photosynthesis were enriched among GRP7 target mRNAs that were bound under mock conditions or under both mock and ABA conditions, but not among those bound solely under ABA conditions (Fig. 6d). Notably, the translational efficiency of GRP7 target mRNAs significantly decreased in the *grp7grp8^{CR}-A* mutant compared to Col-0, under both mock and ABA conditions (Fig. 6e). The genes with altered translation efficiency due to GRP7-mediated ABA signaling, including the photosynthesis gene *CAB2*, the stomatal regulation gene *CA2*, and the abiotic stress-responsive gene *FBA2*, were all direct targets of GRP7 identified through CLIP-seq data (Fig. 6f). Further validation using RIP-qPCR confirmed the binding of GRP7 to these genes, while the non-target mRNA *RGS1-HXX1 INTERACTING PROTEIN 1 (RHIP1, At4g26410)* served as a negative control (Fig. 6g). Collectively, these results suggest that GRP7 mediates the regulation of mRNA translation efficiency in response to ABA signaling through its binding to target mRNAs.

Drought regulated translation partly through ABA-GRP7&8

Drought stress induces ABA accumulation and activates ABA-dependent and independent pathways that modify plant morphology for adaptation⁴³. Research indicates that drought can trigger global translational changes^{42,64}. We found both the GRP7-binding targets and genes with GRP7/8-dependent DTE were enriched in the GO term response to water deprivation (Figs. 5k, 6d), indicating a potential role of GRP7 in plant drought response. To investigate whether drought regulates translational changes through the ABA-GRP7&8 pathways, we performed polysome profiling in Col-0, the ABA biosynthetic enzyme mutant *aba2-1*⁶⁵, and *grp7grp8^{CR}-A/G* mutants under PEG treatment for 4 h. PEG treatment significantly reduced the polysome/monosome ratio in Col-0, but this reduction was notably less

pronounced in the *aba2-1* and *grp7grp8^{CR}-A/G* mutants (Fig. 7a and Supplementary Fig. 8), indicating that drought-induced polysome profiling pattern alteration is partially dependent on the ABA-GRP7&8 pathway.

To assess the biological function of GRP7&8-mediated translational regulation under drought stress, we examined the drought tolerance phenotype of the *grp7grp8^{CR}-A* mutant. This mutant exhibited enhanced drought tolerance compared to Col-0, with a significantly higher survival rate following drought exposure (Fig. 7b, c) and a reduced water loss rate in detached leaves (Fig. 7d). Furthermore, we evaluated the translation efficiency of *FBA2*, a gene associated with abiotic stress response⁵³, in Col-0, *aba2-1*, and *grp7grp8^{CR}-A/G* mutants under control and PEG treatment (Fig. 7e). In Col-0, PEG treatment significantly reduced *FBA2* translation efficiency, whereas it remained relatively unchanged in the *aba2-1* and *grp7grp8^{CR}-A/G* mutants (Fig. 7e). Given that *FBA2* is a target of GRP7 (Fig. 6g), these findings suggest that the drought-induced changes in its translation efficiency are partially regulated by the ABA-GRP7&8 pathways (Fig. 7f).

Discussion

Plants, being sessile organisms, constantly face various abiotic stresses. To adapt, they have developed intricate strategies, including precise transcriptional networks that sense harsh environmental cues and redirect developmental programs⁶⁶. Additionally, translational regulation is a crucial pathway that enhances plant growth plasticity^{14,42}. Despite its importance, the signaling mechanisms linking abiotic stress to mRNA translation remain largely unexplored¹³. In this study, we focus on ABA signaling to address this challenge.

ABA is a crucial phytohormone involved in plant growth and stress responses¹⁵. Our research reveals that ABA treatment not only influences mRNA level but also significantly affects mRNA translation efficiency (Fig. 1). Specifically, ABA inhibits global mRNA translation via its core signaling pathway, which includes the receptors PYR/PYL/RCARs, the phosphatase PP2Cs, and the kinase SnRK2s (Fig. 2). Notably, the *snrk2.2/2.3/2.6* mutants exhibit a reduced polysome/monosome ratio compared to Col-0 under mock conditions, likely due to their highly water-sensitive state⁵¹, as drought is also known to inhibit translation⁵². Additionally, a decreased polysome/monosome ratio was observed from two to four days after germination (Supplementary Fig. 9a, b), indicating that early developmental stages significantly influence global translation efficiency. Mutations in *pp2c 3m* and *snrk2.2/2.3/2.6* affected early developmental pace and morphology, while *pyr1pyl1/2/4* mutants showed no significant changes (Supplementary Fig. 9c). The alterations in the polysome/monosome ratio in *pp2c 3m* and *snrk2.2/2.3/2.6* may reflect developmental differences in addition to the direct effects of ABA signaling under mock conditions. Future studies could explore how endogenous developmental cues interact with exogenous stimuli to coordinate the regulation of mRNA translation.

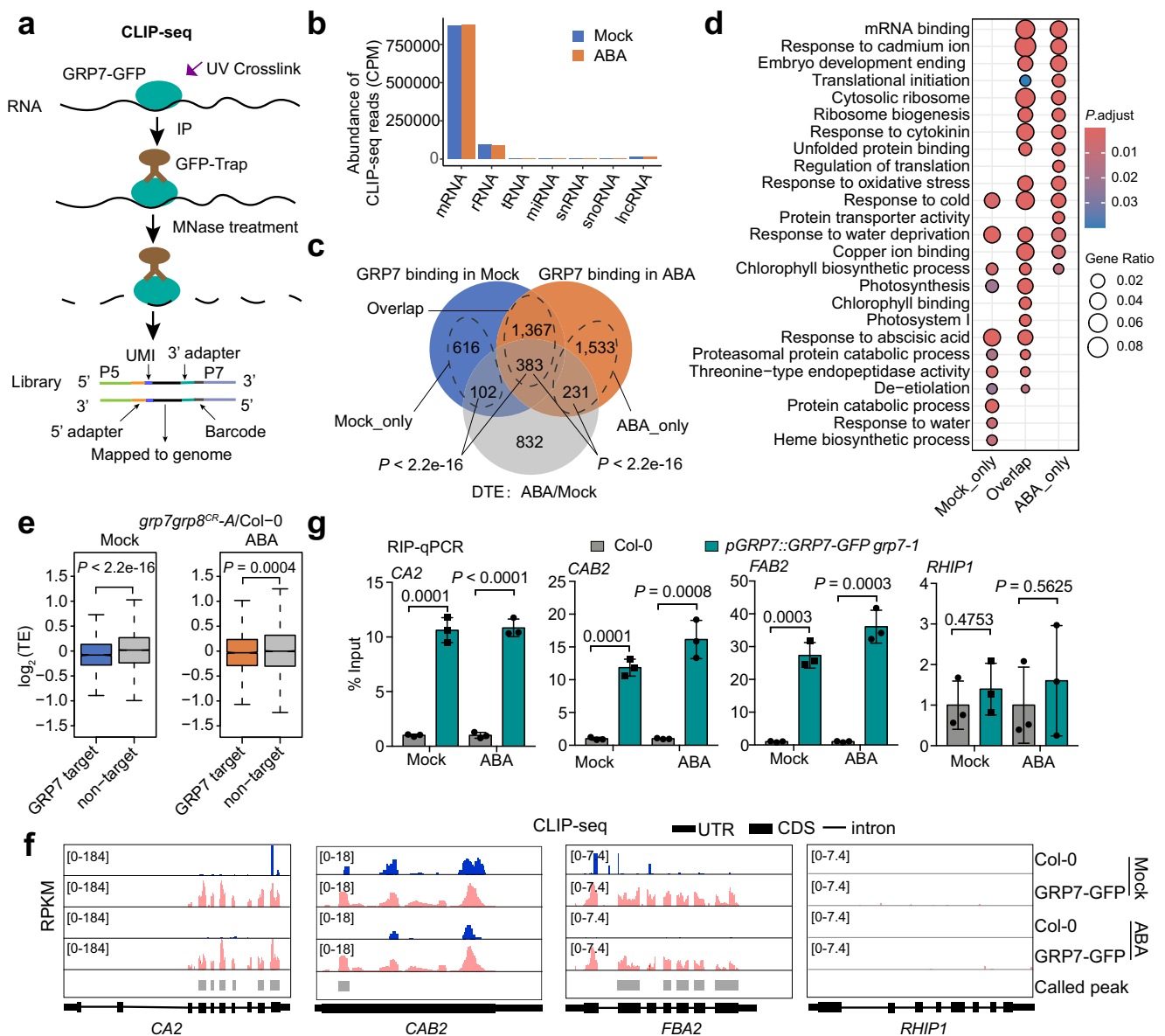


Fig. 6 | GRP7/8 mediates translational regulation of ABA signaling by binding to its target mRNAs. **a** Schematic of the CLIP-seq experiment detecting the direct RNA-binding targets of GRP7. **b** Bar chart showing the abundance of GRP7 CLIP reads mapping to each RNA type upon mock and ABA treatment for 4 h. **c** Venn diagram illustrating the intersection of GRP7-binding genes under mock and ABA treatment with DTE between mock and ABA treatment. The Mock_only, ABA_only and Overlap groups were indicated by gray dashed ellipses. One-sided Hypergeometric tests were used to calculate the P values for the enrichment of genes. **d** GO enrichment of gene sets in (c). P_{adjust} value refers to the Benjamini-Hochberg procedure adjusted P values of one-sided Hypergeometric test. **e** Box plot showing the comparison of $\log_2(\text{TE})$ of *grp7grp8^{CR}-A/Col-0* between GRP7-target mRNAs and non-target mRNAs under mock (left) and ABA treatment (right). In the box plot, borders represent the first and third quartiles, center line denotes median, and whiskers extend to 1.5 times the interquartile range beyond the

quartiles. P value was calculated by two-sided Wilcoxon rank-sum test was used to determine the statistical significance between means of GRP7-target mRNAs and non-target mRNAs. ($n = 2468, 12380, 3514, 11333$ for GRP7 target with mock, non-target with mock, GRP7 target with ABA, non-target with ABA, respectively) **f** IGV showcasing the distribution of CLIP-seq reads across *CA2*, *CAB2*, *FBA2* and *RHIP1* genes in Col-0 and *pGRP7::GRP7-GFP grp7-1* under mock and ABA treatment, Y-axis shows RPKM. Called peak regions were shown under the reads track in gray rectangles. The gene models are depicted with lines representing introns and rectangles of varying thickness indicating the CDS and UTR, respectively. **g** RIP-qPCR analysis of CLIP target mRNAs in *pGRP7::GRP7-GFP grp7-1* and Col-0 under ABA or mock treatment for 4 h. The levels in the GFP-trap precipitate are presented relative to the levels in the input. Data are means \pm S.D. ($n = 3$ biological replicates). P value was calculated by two-sided Student's t test. *RHIP1* as unbound transcripts serve as negative control. Source data are provided as a Source Data file.

While ABA signaling primarily influences transcription through AREB/ABF transcription factors¹, it also modulates translation efficiency via specific RNA-binding proteins, particularly GRP7&8. ABA treatment reduces GRP7&8 protein levels, a process dependent on signaling transduction from PYR/PYL/RCARs to SnRK2s (Fig. 4f, g). Interestingly, the *grp7grp8^{CR}-A/G* mutants exhibit a more sensitive physiological response to ABA, such as inhibited germination, compared to Col-0 (Supplementary Fig. 3b). This suggests that, even when

the translational response is disrupted in *grp7grp8^{CR}-A/G* mutants, normal transcriptional regulation still occurs. To explore how these two regulatory arms coordinate, we assessed the germination phenotypes of Col-0, *snrk2.2/2.3/2.6*, *grp7grp8^{CR}-G*, and the quintuple mutant (*5m*) under varying ABA concentrations (0, 1, and 50 μM) (Fig. 4h, i and Supplementary Fig. 4f, g). Under mock (0 μM) and low ABA concentrations (1 μM), transcriptional regulation via AREB/ABFs appears to drive physiological responses, as the *5m* mutant phenocopied the

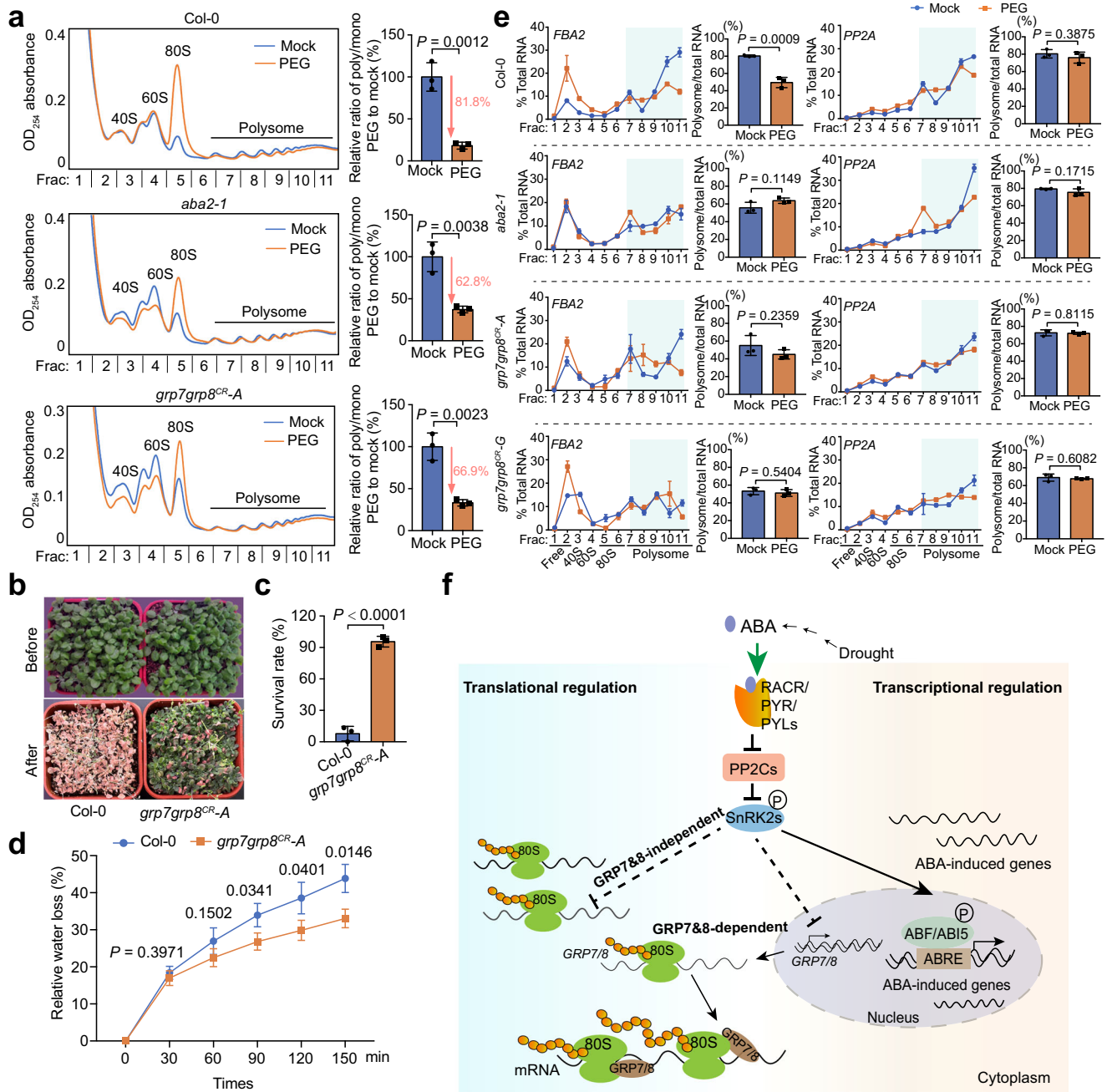


Fig. 7 | Drought regulated translation partly through ABA-GRP7&8. **a** polysome profiles of Col-0, ABA biosynthesis mutant *aba2-1*, and *grp7grp8^{CR-A}* under mock and 15% PEG conditions. Comparison of quantified relative polysome/monosome (poly/mono) ratios of PEG/mock on the right. The pink arrows and numbers represent the decrease in the polysome/monosome ratio under PEG treatment and the percentage of this decrease. The values are means \pm S.D. of $n = 3$ biological replicates. **b** Phenotypes of Col-0, *grp7grp8^{CR-A}* in soil before (top) and after (bottom) drought stress. **c** Survival rate of Col-0 and *grp7grp8^{CR-A}* under drought treatment. Data are means \pm S.D. ($n = 3$ biological replicates, each with 30 plants). **d** Water losses of detached leaves from Col-0 and *grp7grp8^{CR-A}* plants. Data are means \pm S.D. ($n = 3$ biological replicates). **e** Relative RNA level of the *FBA2* and *PP2A* (negative control) across different fractions of polysome profiling in Col-0, *aba2-1* and *grp7grp8^{CR-A/G}* seedlings upon 15% PEG treatment for 4 h. Data are the mean \pm S.D. of three technical replicates from one representative polysome profiling experiment. The proportion of polysome-bound RNA (fractions 7–11, light

green shade) relative to the total RNA were displayed in bar-graph (right). Data are mean \pm S.D. ($n = 3$ biological replicates). **f** Working model for the regulatory role of GRP7 in ABA signal-mediated mRNA translation efficiency regulation. ABA signaling modulates global mRNA translation efficiency through both GRP7&8-dependent and -independent pathways. ABA suppresses GRP7&8 protein levels via its core signaling components—RCAR/PYR/PYLs, PP2Cs, and SnRK2s—ultimately decreasing global mRNA translation. GRP7 associates with ribosomes to influence mRNA translation efficiency and plays a crucial role in ABA-mediated translational regulation by directly binding to its target mRNAs. Furthermore, drought stress regulation of mRNA translation is partially dependent on the ABA-GRP7&8 pathways. In the figure, arrows (\rightarrow) and blunt ends (\perp) indicate activation and inhibition, respectively, while inferred regulations are represented by dashed arrows or blunt ends. Phosphorylated protein. Multiple brown circles represent nascent peptide chains. P value in (**a**, **c**–**e**) were calculated by two-sided Student's t test. Source data are provided as a Source Data file.

snrk2.2/2.3/2.6 phenotype. In contrast, at high concentrations (50 μ M), GRP7&8-mediated translational regulation becomes more influential, evidenced by the increased sensitivity of the *5m* plants compared to *snrk2.2/2.3/2.6*. Overall, ABA signaling operates at both mRNA and translational levels, potentially through distinct pathways downstream of SnRK2s, adapting plant responses to varying ABA concentrations (Fig. 7f).

Upon receiving developmental or environmental signals, translation regulators modulate mRNA translation efficiency, leading to either global reprogramming or gene-specific responses⁶⁷. Under elevated temperatures, GRP7 rapidly forms condensates that recruit target mRNA and components of the translation machinery, such as eukaryotic initiation factor 4E1 (eIF4E1) and cold shock proteins 1 (CSP1) and 3 (CSP3), thereby inhibiting the formation of translation complexes and the translation of heat stress genes⁴¹. In immune responses, GRP7 associates with an active translational complex linked to phosphorylated eIF4E at the mRNA cap, potentially regulating the translation of specific defense-related genes⁴⁰.

In this study, we found that GRP7&8 co-fractionate with the 40S and 60S ribosomal subunits, monosomes, and polysomes, indicating their involvement in maintaining proper translation efficiency for developmental genes in three-day-old seedlings, including those related to photosynthesis and chloroplast biogenesis (Fig. 5k). Following ABA treatment, GRP7&8 protein levels decreased, along with their association with polysomes (Fig. 4), resulting in a decline in global mRNA translation efficiency. The absence of GRP7 and GRP8 significantly disrupts ABA-responsive translation efficiency, with a large portion of DTE affected, highlighting ABA's regulation of translation through GRP7 and GRP8 (Fig. 5). However, ABA treatment still reduces the polysome/monosome ratio in the absence of GRP7&8 (Fig. 3h, i), suggesting that ABA regulates translation through both GRP7&8-dependent and -independent pathways (Fig. 7f). These pathways may function sequentially, with the GRP7&8-independent mechanism initiating the first wave for the translational and transcriptional regulation, including GRP7&8 expression itself, while decreased GRP7&8 levels trigger a secondary wave of translational regulation (Fig. 7f).

Furthermore, the translation efficiency of GRP7-binding targets significantly decreases in plants lacking GRP7&8, suggesting that GRP7&8's regulation of translation efficiency relies on its direct binding to target mRNAs (Fig. 6e). Notably, GRP7 associates with ribosomes even in the absence of RNA binding (Fig. 4a, b and Supplementary Fig. 4b), suggesting that GRP7 may facilitate target mRNA translation by promoting polysome loading. Unlike heat stress, where GRP7 specifically targets several mRNAs, ABA treatment induces a broader reprogramming of mRNA translation efficiency through GRP7&8. Additionally, GRP7's regulation of specific genes may involve different mechanisms, promoting some developmental genes while inhibiting stress-related genes under normal condition.

Interestingly, ABA treatment reduces GRP7&8 protein levels, not through alterations in protein stability, a finding consistent with previous reports³⁵. Our study shows that treatment with 5 μ M ABA in three-day-old seedlings suppresses GRP7&8 mRNA level, as demonstrated by RNA-seq and RT-qPCR analyses (Fig. 4d). This aligns with findings in two-week-old plants treated with 100 μ M ABA⁵⁵ but contrasts with reports of increased GRP7 mRNA levels in 7-day-old plants under 100 μ M ABA³⁵. Previous studies indicated that ABA treatment elevates levels of alternative spliced GRP7 (as_GRP7), which contains a premature stop codon, while decreasing levels of fully spliced GRP7 RNA (fs_GRP7)³⁵. Our results reveal a decline in both as_GRP7 and fs_GRP7 levels in three-day-old seedlings treated with 5 μ M ABA (Supplementary Fig. 10), alongside a decrease in GRP7 translation efficiency (Fig. 4e). We speculate that variations in developmental stages and ABA concentrations may lead to differential regulation of GRP7 by ABA

treatment. Further investigation into how ABA regulates GRP7 and GRP8 from multiple perspectives would be valuable.

Given that abiotic stresses like drought and salinity can trigger ABA biosynthesis and influence plant development^{5,6}, we used drought as a model to explore its effects. Our findings suggest that drought partially relies on the ABA-GRP7&8 modules to modulate mRNA translation. Translational regulation responds more rapidly to environmental stresses than transcriptional regulation, enabling swift adaptation⁶⁸. Thus, investigating the comparative roles of transcription and translation regulation in the rapid response and long-term adaptation to drought through transcriptome and translome analyses at different time points will be an intriguing area for further study.

Methods

Plant materials and growth conditions

Arabidopsis thaliana plants used in this study were in the Col-0 background. The seeds were sterilized using a 75% ethanol solution with 0.1% Triton X-100. After sterilization, they were sown onto plates with half-strength Murashige and Skoog (MS) medium, which had been adjusted to a pH of 5.7 and supplemented with 1% (w/v) sucrose and 0.8% (w/v) agar. These plates were then placed in a dark cold room for stratification at 4 °C for a period of three days. Following this, the plates were moved to a light incubator under long-day conditions (LD, 16 h of light and 8 h of darkness) at 22 °C, and subject to mock, ABA or PEG treatment at ZT10. For ABA treatment, three-day-old seedlings were transferred onto filter paper that had been moistened with 1/2 MS liquid medium containing 5 μ M ABA or an equivalent volume of mock solution. They were then incubated under the same long-day conditions at 22 °C for 4 h. For PEG treatment, 6-days-old seedlings were transferred onto filter paper that had been moistened with 1/2 MS liquid medium containing 15% PEG or an equivalent volume of mock solution. They were then incubated under the same long-day conditions at 22 °C for 4 h. The seedlings were then gently dried and flash-frozen in liquid nitrogen. The samples were stored at -80 °C for further analysis.

To generate *pACTIN2::FLAG-eL18y*, the *eL18y* CDS sequence was amplified by PCR using cDNA as a template. The resulting DNA fragment was ligated into the pCambia3301 vector driven by the *ACTIN2* promoter from *Arabidopsis thaliana*. The resulting construct was transformed into *Agrobacterium tumefaciens* GV3101 and transferred to Col-0 plants using the floral dip method. The *grp7grp8^{CR}-A*, *grp7grp8^{CR}-G*, *grp8^{CR}-A* and *grp8^{CR}-G* mutants were created by CRISPR/Cas9 editing. *grp7-1* (SALK_039556) mutant described previously⁷. The *pp2c* triple mutant (*3m*) (*abi1-2abi2-2hab1-1*)⁴⁸, *snrk2.2/2.3/2.6⁵⁰*, *aba2-1⁶⁹* and *pyr1pyl1/2/4⁴⁶* were described previously. The *pGRP7::GRP7-GFP* *grp7-1* complementary line⁵⁶ was described previously. The *snrk2.2/2.3/2.6* *grp7grp8^{CR}-G* quintuple mutant (*5m*) was established by crossing *snrk2.2/2.3/2.6* and *grp7grp8^{CR}-G*. The primers used for identification of the mutations are listed in Supplementary Data 11.

Physiological experiments

For the germination assay⁷⁰, approximately 50 seeds were sown on 1/2 MS medium supplemented with varying concentrations of ABA. The plates were initially incubated at 4 °C for 3 days and then transferred to a light incubator under LD conditions for a subsequent 15-day growth period to assess seed germination rates. Photographs were taken continuously throughout this period. Seed germination was defined as the radicle rupture of the seed coat. Green cotyledons were defined as seedlings with expanded cotyledons. The experiment was performed with three replicates.

For the drought stress tolerance⁴⁸, 7-days-old seedlings were transplanted into pots and cultivated under normal long-day growth conditions for a period of two weeks. Subsequently, drought stress was imposed by withholding water from the seedlings for an additional two weeks. The drought phenotypes were photographed three days

following rehydration. To assess water loss in detached leaves, 7-day-old seedlings were transplanted into soil and cultivated for 3 weeks under a 16-h light/8-h dark photoperiod. The fifth true leaves from plants grown under same conditions were selected. The leaves were cut, placed on weighing paper and weighted immediately. Four leaves were used for each genotype and placed on the same piece of weighing paper. The leaves were then returned to normal growth conditions. The relative water loss rate was calculated as the ratio of water loss to the initial fresh weight.

Polysome profiling analysis

Arabidopsis thaliana polysomes were fractionated over sucrose gradients as described with minor modifications¹⁹. In brief, three-day-old seedlings were treated with 5 μ M ABA for 4 h and then ground in liquid nitrogen followed by resuspension in polysome extraction buffer containing 200 mM Tris-HCl pH 9.0, 200 mM KCl, 35 mM MgCl₂, 25 mM EGTA, 1% sodium deoxycholate, 1% Detergent mix (20% Brij, 20% Triton X-100, 20% Igepal CA630, 20% Tween 20), 1% Polyoxyethylene 10 tridecyl ether (PTE), 5 mM DTT, 1 mM PMSF, 50 μ g/mL cycloheximide, 50 μ g/mL chloramphenicol, and 80 U/mL SUPERase-In RNase Inhibitor (Invitrogen Cat# AM2694). The supernatant was loaded onto a 10%–50% sucrose gradient (10 \times Sucrose salt buffer: 400 mM Tris-HCl pH: 8.4, 200 mM KCl, 100 mM MgCl₂) and spun in a Beckman SW41Ti rotor at 33,500 rpm for 3 h at 4 °C. We collected 11 fractions by a gradient fractionator. For RNase A treatment⁷¹, SUPERase-In RNase Inhibitor was omitted from the polysome extraction buffer. After lysis, 1 μ L of RNase A (Invitrogen, catalog no. AM2270) was added to the lysate. For EDTA treatment⁷¹, lysates were layered on a linear sucrose gradient (10%–50% sucrose (w/v), 25 mM Tris-HCl, pH 7.5, 150 mM NaCl, 50 mM EDTA, and 1 mM DTT).

For polysome RNA extraction¹⁹, 600 μ L of phenol–chloroform–isoamyl alcohol were pipetted into a 600 μ L sample of different fractions. Then, 15 μ L of 10% SDS, 12 μ L of 0.5 M EDTA (pH 8.0), and 3 μ L of 1 M DTT were added to each tube and mixed thoroughly. The samples were then extracted and centrifuged at 12,000 *g* for 15 minutes. The supernatant (500 μ L) was transferred to a fresh tube. RNA was precipitated by adding 50 μ L of 3 M sodium acetate (pH 5.2) and 500 μ L of isopropanol. The RNA was subjected to reverse transcription and qPCR analysis.

For polysome protein extraction, we added 900 μ L of methanol, 220 μ L of trichloromethane, and 600 μ L of H₂O to a 600 μ L sample of different fractions. The mixture was then well mixed and allowed to stand for 10 minutes at room temperature before being centrifuged at 18,000 *g* for 5 minutes at room temperature. After carefully removing the upper aqueous phase, 600 μ L of methanol were added to each tube, mixed well, and centrifuged again at 18,000 *g* for 5 min at room temperature. Finally, 50 μ L of protein loading buffer was added to the precipitate and incubated at 95 °C for 10 minutes. The sample is now ready for subsequent experiments, such as Western blotting.

SUnSET assay

SUnSET assay is modified from a previous protocol²⁹. Briefly, three-day-old seedlings were treated with mock and 5 μ M ABA for 3.5 h, after which 50 μ M puromycin was applied to the samples for 30 minutes. The seedlings were ground in liquid nitrogen, to which 2 \times SDS loading buffer was subsequently added. After vigorous mixing, the lysates were boiled at 95 °C for 10 minutes. Puromycin-labeled proteins were detected by western blot probed with an anti-puromycin antibody (EMD Millipore, MABE343, 1:3000 dilution).

RNA immunoprecipitation (RIP) and qPCR analyses

RIP was performed as described previously with some modifications⁷². One gram of three-day-old seedlings were treated with mock and 5 μ M ABA for 4 h and then ground in liquid nitrogen followed by cross-linking twice at 600 mJ/cm² in a UVP crosslinker (Analytik jena).

Samples were solubilized using 2 mL of extraction buffer, composed of 50 mM Tris-HCl pH 8.0, 150 mM NaCl, 4 mM MgCl₂, 0.1% Igepal CA-630, 5 mM DTT, 0.1% SDS, 1 mM PMSF, protease inhibitor, and 80 U/mL SUPERase-In RNase Inhibitor. 100 μ L supernatant was used as input. RNA-GRP7-GFP complexes were enriched from the supernatant by immunoprecipitation with GFP-trap beads for 2 h at 4 °C under constant rotation. The GFP-Trap beads (Lablead, GNM-25-1000) were then washed four times with a washing buffer containing 50 mM Tris-HCl at pH 8.0, 150 mM NaCl, 2 mM EDTA, 1% Igepal CA-630, and 0.1% SDS. To elute the protein–RNA complexes, the beads were incubated at room temperature for 10 minutes with gentle rotation in 50 μ L of RIP elution buffer, which contained 100 mM Tris-HCl at pH 7.4, 100 mM NaCl, 10 mM EDTA, 1% SDS, and 80 U/mL RNase inhibitor. The protein was degraded by proteinase K, and co-precipitated RNAs were eluted by 1 mL TRIzol of RNA extraction reagent. The RNA sample was incubated with DNase I and reverse-transcribed using cDNA synthesis kit (TIANGEN, KR116) for qPCR. In parallel, input samples were used for quantification. The primers used for qPCR are listed in Supplementary Data 11.

Ribosome profiling (Ribo-seq)

Ribosome profiling experiment was performed as previous reported with some modifications^{73,74}. In brief, three-day-old seedlings were treated with 5 μ M ABA for 4 h and then ground in liquid nitrogen followed by resuspension in 600 μ L ice-cold lysis buffer. Upon clarifying the lysate by centrifugation for 10 minutes at 20,000 *g* at 4 °C, the soluble supernatant was recovered. 6 μ L of RNase I (100 U/ μ L) were added to 600 μ L lysate and incubated for 45 minutes at room temperature with gentle mixing. 10 μ L SUPERase-In RNase Inhibitor was then added to stop nuclease digestion. Meanwhile, MicroSpin S-400 HR columns (GE Healthcare Cat# 275140-01) were equilibrated with 3 mL of mammalian polysome buffer by gravity flow and emptied by centrifugation at 600 *g* for 4 minutes. The digested lysate was immediately loaded on the column and eluted from the column by centrifugation at 600 *g* for 2 minutes. The RNA was extracted from the flow-through using Trizol (Thermo Fisher, 15596018CN). The ribosomal RNA fragments were removed using the Ribo-off rRNA depletion kit (Plant) (Vazyme, N409) and separated on a 15% denaturing urea-PAGE gel. The size ranges from 27 nt to 30 nt was cut and thus obtained RNA fragments were subjected into library generation using Smarter smRNA-Seq kit (Takara Cat# 635031).

Crosslinking and Immunoprecipitation Sequencing (CLIP-seq)

CLIP was performed as previously described with minor modifications^{63,72}. In brief, three-day-old seedlings were treated with mock and 5 μ M ABA for 4 h and seedling samples (approximately 1 g) were harvested. Seedling samples were then rapidly frozen in liquid nitrogen and ground into a fine powder, which was crosslinked twice with 254 nm ultraviolet light at a dose of 600 mJ/cm² in the mortar pre-cooled with liquid nitrogen. The sample powder was suspended in lysis buffer, treated with DNase I. The resulting lysate was cleared by centrifugation, after which immunoprecipitation was performed using GFP-Trap beads. After immunoprecipitation, the RNA-protein complex was washed extensively several times with high-salt wash buffer and partially digested by micrococcal nuclease (2 \times 10⁻⁵ U/ μ L, Takara, 2910 A)²⁷. The digested RNA was treated with polynucleotide kinase to remove the 3'-terminal phosphate from RNA. The immunoprecipitated RNAs were ligated with RNA adaptors (biotin labeling) and the resulting complex was eluted using SDS loading buffer. Next, 10% of the eluate was separated on a 4–12% NuPAGE (Thermo Fisher) gel and transferred to a nitrocellulose membrane for biotin staining to assess enrichment of the RNA bound by target protein. The remaining 90% of the eluate was run in parallel. The nitrocellulose membrane was excised and RNA was released from the complex by proteinase K treatment. RNA was further purified and reverse-transcribed using

AffinityScript reverse transcriptase (Agilent) with a primer complementary to the RNA adaptor to produce complementary DNA. The cDNA was purified and a DNA adapter was ligated to the 3' end. The final library was amplified from the cDNA by Q5 HotStart DNA polymerase using primers specific to adaptors. The resulting PCR products were purified and resolved on a 3% agarose gel, and fragments in the size range of 150 to 200 bp were recovered from the gel and used for paired-end Illumina (PE150) sequencing.

Immunoprecipitation Mass Spectrometry (IP-MS) assay

Immunoprecipitation of Flag-eL18y proteins from three-day-old *pACTIN2::FLAG-eL18y* and Col-0 (negative control) seedlings was performed as previously described with some modifications⁷¹. Proteins were solubilized from plant powder using buffer A (25 mM Tris-HCl pH 7.5, 150 mM NaCl, 15 mM MgCl₂, 1 mM DTT, 8% glycerol, 1% Triton X-100, 0.5% sodium deoxycholate, 100 µg/mL Cycloheximide (CHX), 100 U/mL SUPERase-In RNase Inhibitor, 25 U/mL Turbo DNase, Protease Inhibitor). Anti-FLAG M2 magnetic beads (Sigma-Aldrich, Cat#M8823) were used to immunoprecipitate Flag-eL18y from the protein extracts. IP samples were first washed three times for 5 minutes each at 4 °C with buffer B (25 mM Tris-HCl pH 7.5, 150 mM NaCl, 15 mM MgCl₂, 1 mM DTT, 1% Triton X-100, 0.5% sodium deoxycholate, 100 µg/mL CHX). Afterward, the beads were washed three times for 5 minutes each at 4 °C using buffer C (25 mM Tris-HCl pH 7.5, 300 mM NaCl, 15 mM MgCl₂, 1 mM DTT, 1% Triton X-100, 0.5% sodium deoxycholate, 100 µg/mL CHX). The resulting complex was eluted using SDS loading buffer. The Coomassie-stained gel strips were subjected to destaining, followed by reduction with DTT and alkylation with iodoacetamide. After these treatments, the gel strips were digested with trypsin overnight. Subsequently, the peptides were extracted in multiple steps using different concentrations of acetonitrile, which subjected to MS analyses by Liquid Chromatography–Mass Spectrometry (LC-MS, nanoLC-Q EXACTIVE, Thermo Scientific). There were two biological replicates for both the experimental group and the control group.

Western blot assay

For western blot analysis, protein samples were resolved by SDS-PAGE and then transferred onto a PVDF membrane. The membrane was blocked with 5% milk in PBST (containing 0.1% Tween-20) for 1 hour at room temperature. Subsequently, the membrane was incubated with primary antibodies: anti-GRP7 (1:2000 dilution), anti-Flag (Sigma, Cat#F1804, 1:5000 dilution), anti-eS6z (PHYTOAB, Cat#PHY2025A, 1:2000 dilution) antibody and anti-GAPDH (Proteintech, Cat#60004, 1:5000). Anti-actin antibody (LabLead, Cat#BPO101, 1:5000 dilution) was used as internal control. Immunoblotting was done by using the enhanced chemiluminescence (ECL) system.

Bioinformatics analysis

Raw reads of RNA-seq, Ribo-seq, and CLIP-seq were filtered by fastp v0.20.1 for adapters removing, low-quality bases trimming, and reads filtering⁷⁵. RNA-seq reads were filtered with parameter “--detect_adapter_for_pe”, CLIP-seq reads were filtered with parameter “--adapter_sequence TGGAATTCTCGG --adapter_sequence_r2 GATCGTCGGACT”. For Ribo-seq data, only first sequencing reads (*_RI.fq.gz) were used and filtered with parameter “-a AAAAAAAAAA -f 3 -l 16”. The high-quality reads of RNA-seq were mapped to the *Arabidopsis thaliana* genome (TAIR10) using STAR (v2.7.10) with default parameters⁷⁶. The clean reads of Ribo-seq were firstly aligned against the non-coding RNA sequences of *Arabidopsis thaliana* downloaded from Ensembl Plants⁷⁷ using bowtie2 (ref. 78) to produce the unaligned reads. The unaligned reads were mapped to reference genome using STAR with parameters “--outFilterMismatchNmax 2 --outFilterMultimapNmax 1 --outFilterMatchNmin 14 --alignEndsType EndToEnd”. For CLIP-seq data, the clean reads were mapped to reference genome using STAR with no more than two mismatches⁷⁶

and the duplicates in mapped reads were removed using Picard v2.23.3. The overview of RNA-seq, Ribo-seq, and CLIP-seq total reads, filtered read and mapped reads is summarized in Supplementary Data 12.

Two or three replicates bam files were merged using Samtools v1.4 (ref. 79). To normalize and visualize the individual and merged replicate datasets, the BAM files were converted to bigwig files using bamCoverage provided by deepTools v3.3.0 with 1bp bin size and normalized by RPKM (Reads Per Kilobase per Million mapped reads) with parameters “-bs 1 --effectiveGenomeSize 120,000,000 --normalizeUsing RPKM --smoothLength 5” (ref. 80). The number of reads that mapped to each gene was counted using featureCounts v2.0.1 with the parameter “-p -P -B -C” for RNA-seq and default parameters for Ribo-seq⁸¹. The raw counts were further normalized to FPKM (Fragments per kilobase per million mapped reads) for RNA-seq and RPKM (Reads per kilobase per million mapped reads) for Ribo-seq. FPKM or RPKM values of genes were Z-scaled and clustered by k-means method and displayed using R package ComplexHeatmap (v2.4.3) (ref. 82). Gene Ontology enrichment was performed using an R package clusterProfiler v3.18.1 (ref. 83).

The raw counts files of RNA-seq were used as inputs for differential expression analysis by DESeq2 v1.26.0 (ref. 84). We quantified the mapped reads of RNA-seq and Ribo-seq across the 5' UTR, CDS, and 3' UTR regions, then calculated the percentage of reads in each region to determine the distribution ratio of reads in the 5' UTR, CDS, and 3' UTR. The Ribo-TISH toolkit was employed to analyze the distribution of Ribo-seq 5' end counts across the three reading frames within the CDS of all genes, as well as the distribution of Ribo-seq 5' end counts around the start and stop codons of all annotated genes. Only reads located within coding sequences (CDSs) were retained for translation efficiency analyses. Translation efficiency was calculated using the Xtail package (v1.1.5), which employs a Negative Binomial (NB) model to estimate the distributions of both mRNA and ribosome-protected mRNA fragments (RPF)⁸⁵. The analysis includes an evaluation of both the statistical significance and the magnitude of differential translation for each gene. Differential translation efficiency was identified using a threshold of *P*.adjust < 0.05 (Supplementary Data 1, 2, 4–9).

At the mRNA level, 1,018 down-regulated and 1,100 up-regulated genes under ABA treatment in Col-0, which lost their responses in *grp7grp8^{CR}-A* were defined as GRP7-dependent ABA-responsive genes. A total of 2,118 out of 5,248 genes (40.35%) showed GRP7-dependent responses under ABA treatment (Fig. 5g, h). Similarly, 657 genes with down-regulated DTE and 598 genes with up-regulated DTE under ABA treatment in Col-0, which lost their responses in *grp7grp8^{CR}-A*, were defined as GRP7 dependent ABA-responsive genes at translational level. A total of 1,255 out of 1,548 genes (81.07%) showed GRP7-dependent DTE responses under ABA treatment (Fig. 5i, j).

The GRP7 binding sites were identified by performing CLIP-seq peak calling using CLIPper (v0.1.4) with default parameters⁸⁶. Then, bedtools was used to retain the peaks that were identified in both biological replicates⁸⁷. Finally, we defined the peaks that were only identified in IP samples but depleted in negative controls as significant binding sites of GRP7. The GRP7 binding peaks were annotated to the *Arabidopsis thaliana* genome using the “annotatePeak” function in R package ChIPseeker (v1.26.2) (ref. 83) (Supplementary Data 10). The sequences from GRP7 binding peaks were extracted from genome using Biopython module. The motif enrichment analysis of the GRP7 binding sequences were performed using the online MEME Suite (<https://meme-suite.org/meme/doc/overview.html>).

Statistics & Reproducibility

R (<https://cran.r-project.org/version4.0.2>) was used to compute statistics and generate plots if not specified. The Integrative Genomics Viewer (IGV) was used for the visual exploration of genomic data⁸⁸. The intersection between two sets of genes was displayed using the R

package VennDiagram v1.7.3. One-sided Hypergeometric test was used in Figs. 1d, 3d, 3e, 5k, 6c, 6d, Supplementary Figs. 1b, 7d. The Pearson correlation coefficient analysis was used in Supplementary Figs. 1a, 6. The two-sided student's *t*-test was used in Figs. 1f, 2a–e, 3g, 3i, 4c–e, 4g, 5l, 6g, 7a, 7c–e, Supplementary Figs. 2b, 3b, 3c, 8. Two-way ANOVA was used in Figs. 3k, 4i, Supplementary Fig. 4g. Two-sided Wilcoxon rank-sum test was used in Fig. 6e. Tukey's HSD multiple comparison test was used in Supplementary Fig. 9b. No statistical method was used to predetermine sample size. No data were excluded from the analyses. The experiments were not randomized. The investigators were not blinded to allocation during experiments and outcome assessment.

Reporting summary

Further information on research design is available in the Nature Portfolio Reporting Summary linked to this article.

Data availability

The raw sequence data of RNA-seq, Ribo-seq, and CLIP-seq generated in this study have been deposited in the Genome Sequence Archive (<https://bigd.big.ac.cn/gsa>)⁸⁹ in National Genomics Data Center⁹⁰ under accession number CRA012798 [<https://ngdc.cncb.ac.cn/bioproject/browse/PRJCA020137>]. The mass spectrometry proteomics data have been deposited to the ProteomeXchange Consortium via the PRIDE⁹¹ partner repository with the dataset identifier PXD062372. Source data are provided with this paper.

Code availability

Code used for all processing and analysis is available at Github⁹² [<https://doi.org/10.5281/zenodo.15100481>].

References

- Chen, K. et al. Abscisic acid dynamics, signaling, and functions in plants. *J. Integr. Plant Biol.* **62**, 25–54 (2020).
- Vishwakarma, K. et al. Abscisic acid signaling and abiotic stress tolerance in plants: a review on current knowledge and future prospects. *Front. Plant Sci.* **8** (2017).
- Finkelstein, R. Abscisic acid synthesis and response. *Arabidopsis Book* **11**, e0166 (2013).
- Kumar, S. et al. Abscisic acid: Metabolism, transport, crosstalk with other plant growth regulators, and its role in heavy metal stress mitigation. *Front. Plant Sci.* **13**, 972856 (2022).
- Soma, F., Takahashi, F., Yamaguchi-Shinozaki, K. & Shinozaki, K. Cellular phosphorylation signaling and gene expression in drought stress responses: ABA-dependent and ABA-independent regulatory systems. *Plants* **10**, 756 (2021).
- Zhao, C., Zhang, H., Song, C., Zhu, J.-K. & Shabala, S. Mechanisms of plant responses and adaptation to soil salinity. *Innovation* **1**, 100017 (2020).
- Santiago, J. et al. Structural insights into PYR/PYL/RCAR ABA receptors and PP2Cs. *Plant Sci.* **182**, 3–11 (2012).
- Santiago, J. et al. The abscisic acid receptor PYR1 in complex with abscisic acid. *Nature* **462**, 665–668 (2009).
- Hirayama, T. & Umezawa, T. The PP2C-SnRK2 complex: the central regulator of an abscisic acid signaling pathway. *Plant Signal Behav.* **5**, 160–163 (2010).
- Ng, L. M., Melcher, K., Teh, B. T. & Xu, H. E. Abscisic acid perception and signaling: structural mechanisms and applications. *Acta Pharmacologica Sin.* **35**, 567–584 (2014).
- Guo, J. et al. Involvement of *Arabidopsis* RACK1 in protein translation and its regulation by abscisic acid. *Plant Physiol.* **155**, 370–383 (2011).
- Bi, C. et al. *Arabidopsis* translation initiation factors eIF iso4G1/2 link repression of mRNA cap-binding complex eIF iso4F assembly with RNA-binding protein SOAR 1-mediated ABA signaling. *N. Phytologist* **223**, 1388–1406 (2019).
- Wu, H. Y. L., Jen, J. & Hsu, P. Y. What, where, and how: Regulation of translation and the translational landscape in plants. *Plant Cell* **36**, 1540–1564 (2024).
- Merchante, C., Stepanova, A. N. & Alonso, J. M. Translation regulation in plants: an interesting past, an exciting present and a promising future. *Plant J.* **90**, 628–653 (2017).
- Zaher, H. S. & Green, R. Fidelity at the molecular level: Lessons from protein synthesis. *Cell* **136**, 746–762 (2009).
- Browning, K. S. & Bailey-Serres, J. Mechanism of cytoplasmic mRNA Translation. *Arabidopsis Book* **13**, e0176 (2015).
- Scarpin, M. R. An updated nomenclature for plant ribosomal protein genes. *Plant Cell* **35**, 640–643 (2023).
- Pelletier, J., Thomas, G. & Volarevic, S. Ribosome biogenesis in cancer: new players and therapeutic avenues. *Nat. Rev. Cancer* **18**, 134–134 (2018).
- Missra, A. & von Arnim, A. G. In *plant circadian networks* Vol. 1158 (ed D. Staiger) 157–174 (Springer New York, 2014).
- Zuccotti, P. & Modelska, A. In *post-transcriptional gene regulation* Vol. 1358 (ed Erik D.) 59–69 (Springer New York, 2016).
- Ingolia, N. T., Ghaemmaghami, S., Newman, J. R. S. & Weissman, J. S. Genome-wide analysis in vivo of translation with nucleotide resolution using ribosome profiling. *Science* **324**, 218–223 (2009).
- Liu, M.-J. et al. Translational landscape of photomorphogenic *Arabidopsis*. *Plant Cell* **25**, 3699–3710 (2013).
- Zhou, Y. et al. Plant HEM1 specifies a condensation domain to control immune gene translation. *Nat. Plants* **9**, 289–301 (2023).
- Hsu, P. Y. et al. Super-resolution ribosome profiling reveals unannotated translation events in *Arabidopsis*. *Proc. Natl Acad. Sci. USA* **113**, <https://doi.org/10.1073/pnas.1614788113> (2016).
- Brar, G. A. & Weissman, J. S. Ribosome profiling reveals the what, when, where and how of protein synthesis. *Nat. Rev. Mol. Cell Biol.* **16**, 651–664 (2015).
- Guo, Y. et al. The translational landscape of bread wheat during grain development. *The Plant Cell*, koad075 (2023).
- Zhao, T. et al. Impact of poly(A)-tail G-content on *Arabidopsis* PAB binding and their role in enhancing translational efficiency. *Genome Biol.* **20**, 189 (2019).
- Huang, Y.-H. et al. A translational regulator MHZ9 modulates ethylene signaling in rice. *Nat. Commun.* **14**, 4674 (2023).
- Chen, T. et al. Global translational induction during NLR-mediated immunity in plants is dynamically regulated by CDC123, an ATP-sensitive protein. *Cell Host Microbe* **31**, 334–342.e335 (2023).
- Lee, M.-H. RNA-binding proteins. *WormBook* <https://doi.org/10.1895/wormbook.1.79.1> (2006).
- Mateos, J. L. & Staiger, D. Toward a systems view on RNA-binding proteins and associated RNAs in plants: Guilt by association. *Plant Cell* **35**, 1708–1726 (2023).
- Ma, L. et al. Roles of Plant Glycine-Rich RNA-binding proteins in development and stress responses. *Int. J. Mol. Sci.* **22**, 5849 (2021).
- Kwak, K. J., Kim, Y. O. & Kang, H. Characterization of transgenic *Arabidopsis* plants overexpressing GR-RBP4 under high salinity, dehydration, or cold stress. *J. Exp. Bot.* **56**, 3007–3016 (2005).
- Streitner, C. et al. An hnRNP-like RNA-binding protein affects alternative splicing by in vivo interaction with transcripts in *Arabidopsis thaliana*. *Nucleic Acids Res.* **40**, 11240–11255 (2012).
- Wang, L. et al. RALF1-FERONIA complex affects splicing dynamics to modulate stress responses and growth in plants. *Sci. Adv.* **6**, eaaz1622 (2020).
- Kim, J. S. et al. Glycine-rich RNA-binding protein7 affects abiotic stress responses by regulating stomata opening and closing in *Arabidopsis thaliana*. *Plant J.* **55**, 455–466 (2008).
- Xiao, J. et al. AtJAC1 regulates nuclear accumulation of GRP7, influencing RNA Processing of FLC antisense transcripts and flowering time in *Arabidopsis*. *Plant Physiol.* **169**, 2102–2117 (2015).

38. Lewinski, M. et al. *Arabidopsis thaliana* GLYCINE RICH RNA-BINDING PROTEIN 7 interaction with its iCLIP target *LHCB1.1* correlates with changes in RNA stability and circadian oscillation. *Plant J.* **118**, 203–224 (2024).
39. Karimi, H. Z., Baldrich, P., Rutter, B. D., Meyers, B. C. & Innes, R. W. *Arabidopsis* apoplastic fluid contains sRNA- and circular RNA-protein complexes that are located outside extracellular vesicles. *Plant Cell* **34**, 1863–1881 (2022).
40. Nicaise, V. et al. Pseudomonas HopU1 modulates plant immune receptor levels by blocking the interaction of their mRNAs with GRP7. *EMBO J.* **32**, 701–712 (2013).
41. Xu, F. et al. Phase separation of GRP7 facilitated by FERONIA-mediated phosphorylation inhibits mRNA translation to modulate plant temperature resilience. *Mol. Plant* **17**, 460–477 (2024).
42. Son, S. & Park, S. R. Plant translational reprogramming for stress resilience. *Front. Plant Sci.* **14**, 1151587 (2023).
43. Shinozaki, K. & Yamaguchi-Shinozaki, K. Functional genomics in plant abiotic stress responses and tolerance: From gene discovery to complex regulatory networks and their application in breeding. *Proc. Jpn. Acad., Ser. B* **98**, 470–492 (2022).
44. Xu, D. et al. Cellulose defects in the *Arabidopsis* secondary cell wall promote early chloroplast development. *Plant J.* **101**, 156–170 (2020).
45. Yokotani, N. et al. A novel chloroplast protein, CEST induces tolerance to multiple environmental stresses and reduces photo-oxidative damage in transgenic *Arabidopsis*. *J. Exp. Bot.* **62**, 557–569 (2011).
46. Yu, F. et al. ESCRT-I Component VPS23A Affects ABA signaling by recognizing ABA receptors for endosomal degradation. *Mol. Plant* **9**, 1570–1582 (2016).
47. Park, S.-Y. et al. Abscisic acid inhibits type 2C protein phosphatases via the PYR/PYL family of START proteins. *Science* **324**, 1068–1071 (2009).
48. Wang, K. et al. EAR1 negatively regulates ABA signaling by enhancing 2C protein phosphatase activity. *Plant Cell* **30**, 815–834 (2018).
49. Rubio, S. et al. Triple loss of function of protein phosphatases type 2C leads to partial constitutive response to endogenous abscisic acid. *Plant Physiol.* **150**, 1345–1355 (2009).
50. Wang, J. et al. Tyrosylprotein sulfotransferase suppresses ABA signaling via sulfation of SnRK2.2/2.3/2.6. *J. Integr. Plant Biol.* **65**, 1846–1851 (2023).
51. Fujii, H. & Zhu, J.-K. *Arabidopsis* mutant deficient in 3 abscisic acid-activated protein kinases reveals critical roles in growth, reproduction, and stress. *PNAS* **106**, 8380–8385 (2009).
52. Kawaguchi, R., Williams, A. J., Bray, E. A. & Bailey-Serres, J. Water-deficit-induced translational control in *Nicotiana tabacum*. *Plant, Cell Environ.* **26**, 221–229 (2003).
53. Lu, W. et al. Identification and characterization of fructose 1,6-bisphosphate aldolase genes in *Arabidopsis* reveal a gene family with diverse responses to abiotic stresses. *Gene* **503**, 65–74 (2012).
54. Sasaki, K. et al. *Arabidopsis* COLD SHOCK DOMAIN PROTEIN 2 influences ABA accumulation in seed and negatively regulates germination. *Biochemical Biophysical Res. Commun.* **456**, 380–384 (2015).
55. Cao, S., Jiang, L., Song, S., Jing, R. & Xu, G. AtGRP7 is involved in the regulation of abscisic acid and stress responses in *Arabidopsis*. *Cell. Mol. Biol. Lett.* **11**, 526–535 (2006).
56. Meyer, K. et al. Adaptation of iCLIP to plants determines the binding landscape of the clock-regulated RNA-binding protein AtGRP7. *Genome Biol.* **18**, 204 (2017).
57. Streitner, C. et al. The small glycine-rich RNA binding protein AtGRP7 promotes floral transition in *Arabidopsis thaliana*. *Plant J.* **56**, 239–250 (2008).
58. Ogunkolade, B. W. et al. BORIS/CTCFL is an RNA-binding protein that associates with polysomes. *BMC Cell Biol.* **14**, 52 (2013).
59. Pan, W. et al. The UBC27–AIRP3 ubiquitination complex modulates ABA signaling by promoting the degradation of ABI1 in *Arabidopsis*. *Proc. Natl Acad. Sci.* **117**, 27694–27702 (2020).
60. Ferguson, L. et al. Streamlined and sensitive mono- and di-ribosome profiling in yeast and human cells. *Nat. Methods* **20**, 1704–1715 (2023).
61. Tunney, R. et al. Accurate design of translational output by a neural network model of ribosome distribution. *Nat. Struct. Mol. Biol.* **25**, 577–582 (2018).
62. Xu, D. et al. Response of the organellar and nuclear (post)transcriptomes of *Arabidopsis* to drought. *Front. Plant Sci.* **14**, 1220928 (2023).
63. Van Nostrand, E. L. et al. Robust transcriptome-wide discovery of RNA-binding protein binding sites with enhanced CLIP (eCLIP). *Nat. Methods* **13**, 508–514 (2016).
64. Lei, L. et al. Ribosome profiling reveals dynamic translational landscape in maize seedlings under drought stress. *Plant J.* **84**, 1206–1218 (2015).
65. Li, J., Yao, S., Kim, S.-C. & Wang, X. Lipid phosphorylation by a diacylglycerol kinase suppresses ABA biosynthesis to regulate plant stress responses. *Mol. Plant* **17**, 342–358 (2024).
66. Song, L. et al. A transcription factor hierarchy defines an environmental stress response network. *Science* **354**, aag1550–aag1550 (2016).
67. Yuan, S., Zhou, G. & Xu, G. Translation machinery: the basis of translational control. *J. Genet. Genomics* **51**, 367–378 (2024).
68. Zhong, J. et al. Transfer RNAs mediate the rapid adaptation of *Escherichia coli* to oxidative stress. *PLOS Genet.* **11**, e1005302 (2015).
69. Fu, J. et al. A mechanism coordinating root elongation, endodermal differentiation, redox homeostasis and stress response. *Plant J.* **107**, 1029–1039 (2021).
70. Yang, C. et al. ABI5–FLZ13 module transcriptionally represses growth-related genes to delay seed germination in response to ABA. *Plant Commun.* **4**, 100636 (2023).
71. Simsek, D. et al. The mammalian ribo-interactome reveals ribosome functional diversity and heterogeneity. *Cell* **169**, 1051–1065.e1018 (2017).
72. Tong, J. et al. ALBA proteins confer thermotolerance through stabilizing HSF messenger RNAs in cytoplasmic granules. *Nat. Plants* **8**, 778–791 (2022).
73. Tang, Y. et al. OsNSUN2-mediated 5-methylcytosine mRNA modification enhances rice adaptation to high temperature. *Developmental Cell* **53**, 272–286.e277 (2020).
74. Calviello, L. et al. Detecting actively translated open reading frames in ribosome profiling data. *Nat. Methods* **13**, 165–170 (2016).
75. Chen, S., Zhou, Y., Chen, Y. & Gu, J. fastp: an ultra-fast all-in-one FASTQ preprocessor. *Bioinformatics* **34**, i884–i890 (2018).
76. Dobin, A. et al. STAR: ultrafast universal RNA-seq aligner. *Bioinformatics* **29**, 15–21 (2013).
77. Cunningham, F. et al. Ensembl 2022. *Nucleic Acids Res.* **50**, D988–D995 (2022).
78. Langmead, B. & Salzberg, S. L. Fast gapped-read alignment with Bowtie 2. *Nat. Methods* **9**, 357–359 (2012).
79. Danecek, P. et al. Twelve years of SAMtools and BCFtools. *Giga-Science* **10**, giab008 (2021).
80. Ramírez, F., Dündar, F., Diehl, S., Grüning, B. A. & Manke, T. deepTools: a flexible platform for exploring deep-sequencing data. *Nucleic Acids Res.* **42**, W187–W191 (2014).
81. Liao, Y., Smyth, G. K. & Shi, W. featureCounts: an efficient general purpose program for assigning sequence reads to genomic features. *Bioinformatics* **30**, 923–930 (2014).
82. Gu, Z., Eils, R. & Schlesner, M. Complex heatmaps reveal patterns and correlations in multidimensional genomic data. *Bioinformatics* **32**, 2847–2849 (2016).

83. Yu, G., Wang, L.-G., Han, Y. & He, Q.-Y. clusterProfiler: an R package for comparing biological themes among gene clusters. *OMICS: A J. Integr. Biol.* **16**, 284–287 (2012).
84. Love, M. I., Huber, W. & Anders, S. Moderated estimation of fold change and dispersion for RNA-seq data with DESeq2. *Genome Biol.* **15**, 550 (2014).
85. Xiao, Z., Zou, Q., Liu, Y. & Yang, X. Genome-wide assessment of differential translations with ribosome profiling data. *Nat. Commun.* **7**, 11194 (2016).
86. Lovci, M. T. et al. Rbfox proteins regulate alternative mRNA splicing through evolutionarily conserved RNA bridges. *Nat. Struct. Mol. Biol.* **20**, 1434–1442 (2013).
87. Quinlan, A. R. & Hall, I. M. BEDTools: a flexible suite of utilities for comparing genomic features. *Bioinformatics* **26**, 841–842 (2010).
88. Robinson, J. T. et al. Integrative genomics viewer. *Nat. Biotechnol.* **29**, 24–26 (2011).
89. Chen, T. et al. The genome sequence archive family: Toward explosive data growth and diverse data types. *Genomics, Proteom. Bioinforma.* **19**, 578–583 (2021).
90. Partners, C.-N. M., et al. Database resources of the national genomics data center, china national center for bioinformatics in 2022. *Nucleic Acids Res.* **50**, D27–D38 (2022).
91. Perez-Riverol, Y. et al. The PRIDE database at 20 years: 2025 update. *Nucleic Acids Res.* **53**, D543–D553 (2025).
92. Wu, Y. & Yu, X. Transfer learning enables identification of multiple types of RNA modifications using nanopore direct RNA sequencing. Zenodo <https://doi.org/10.5281/zenodo.15100481> (2025).

Acknowledgements

We thank Professor Z.-Z. Gong (CAU) provided *pp2c 3 m*, Professor J.-G. Huang (SDAU) and Professor J.-K. Zhu (SUSTC) provided *snrk2.2/2.3/2.6* seeds, Professor Q. Xie (IGDB, CAS) provides *pyr1-pyl1/2/4* seeds, Professor H.-C. Cui (NWAFU) provides *aba2-1* seeds. We thank Professor W. F. Qian (IGDB, CAS) for supporting ribo-seq analysis, Professor J. S. Zhang (IGDB, CAS) for suggestions of CLIP-seq analysis and Dr. C. Y. Liu (IGDB, CAS) for help with Northern blot assay for pre-rRNA processing. We thank Drs. B. Y. Shi (IoG, CAS) and J. Wang (IGDB, CAS) for suggestions on the experimental conduction and data analysis of Ribo-seq assay. We thank Martin Lewinski (Uni Bielefeld) for providing iCLIP data. We thank the Protein Technology Center of the Chinese Academy of Sciences for their assistance with mass spectrometry. This research is supported by Beijing Natural Science Foundation Outstanding Youth Project (JQ23026), the National Key Research and Development Program of China (2021YFD1201500), the National Natural Science Foundation of China (32170581 and 32370587) and the Strategic Priority Research Program of the Chinese Academy of Sciences (XDA24010204).

Author contributions

J.X. designed and supervised the research, J.X., J.Z. X.Y. W.-N. S. Y.-X.X. wrote the manuscript. J.Z. did most of the experiments; W.-N.S. Y.-X.X. performed bio-informatics analysis; F.-A.T. constructed *pACTIN2::FLAG-eL18y* and help with polysome profiling assay; C.-S.H. help with CLIP-seq; D.S., Y.-L.D., and X.-F.Y. provided *pGRP7::GRP7-GFP grp7-1* complementary line and put forward valuable advice on the research; C.-S.H, X.Y., D.-Z.W., X.-L.L., X.-F. Y. D.S. and Y.-L.D. revised the manuscript; J.Z., Y.-X.X., J.-C.C., W.-N. S. X.Y. and J.X. prepared all the figures. All authors discussed the results and commented on the manuscript.

Competing interests

The authors declare no competing interests.

Additional information

Supplementary information The online version contains supplementary material available at <https://doi.org/10.1038/s41467-025-59329-6>.

Correspondence and requests for materials should be addressed to Xiang Yu or Jun Xiao.

Peer review information *Nature Communications* thanks Shintaro Iwasaki, who co-reviewed with Naohiro Kawamoto, Guoyong Xu and the other, anonymous, reviewers for their contribution to the peer review of this work. A peer review file is available.

Reprints and permissions information is available at <http://www.nature.com/reprints>

Publisher's note Springer Nature remains neutral with regard to jurisdictional claims in published maps and institutional affiliations.

Open Access This article is licensed under a Creative Commons Attribution-NonCommercial-NoDerivatives 4.0 International License, which permits any non-commercial use, sharing, distribution and reproduction in any medium or format, as long as you give appropriate credit to the original author(s) and the source, provide a link to the Creative Commons licence, and indicate if you modified the licensed material. You do not have permission under this licence to share adapted material derived from this article or parts of it. The images or other third party material in this article are included in the article's Creative Commons licence, unless indicated otherwise in a credit line to the material. If material is not included in the article's Creative Commons licence and your intended use is not permitted by statutory regulation or exceeds the permitted use, you will need to obtain permission directly from the copyright holder. To view a copy of this licence, visit <http://creativecommons.org/licenses/by-nc-nd/4.0/>.

© The Author(s) 2025